

Low-frequency dielectric dispersion of brain tissue due to electrically long neurites

Hiromu Monai

*Department of Computational Intelligence and System Science, Tokyo Institute of Technology, Kanagawa, Japan and
Research Fellow of the Japan Society for the Promotion of Science, Tokyo, Japan*

Masashi Inoue and Hiroyoshi Miyakawa

School of Life Sciences, Tokyo University of Pharmacy and Life Sciences, Tokyo, Japan

Toru Aonishi*

*Department of Computational Intelligence and System Science, Tokyo Institute of Technology, Kanagawa, Japan
(Received 20 August 2012; published 26 December 2012)*

The dielectric properties of brain tissue are important for understanding how neural activity is related to local field potentials and electroencephalograms. It is known that the permittivity of brain tissue exhibits strong frequency dependence (dispersion) and that the permittivity is very large in the low-frequency region. However, little is known with regard to the cause of the large permittivity in the low-frequency region. Here, we postulate that the dielectric properties of brain tissue can be partially accounted for by assuming that neurites are of sufficient length to be “electrically long.” To test this idea, we consider a model in which a neurite is treated as a long, narrow body, and it is subjected to a stimulus created by electrodes situated in the region external to it. With regard to this electric stimulus, the neurite can be treated as a passive cable. Assuming adequate symmetry so that the tissue packed with multiple cables is equivalent to an isolated system consisting of a single cable and a surrounding extracellular resistive medium, we analytically calculate the extracellular potential of the tissue in response to such an externally created alternating-current electric field using a Green’s function that we obtained previously. Our results show that brain tissue modeled by such a cable existing within a purely resistive extracellular medium exhibits a large effective permittivity in the low-frequency region. Moreover, we obtain results suggesting that an extremely large low-frequency permittivity can coexist with weak low-pass filter characteristics in brain tissue.

DOI: [10.1103/PhysRevE.86.061911](https://doi.org/10.1103/PhysRevE.86.061911)

PACS number(s): 87.19.rf, 87.85.dm, 87.50.C–

I. INTRODUCTION

The dielectric properties of brain tissue are important for understanding how neural activity is related to local field potentials (LFPs) and electroencephalograms (EEGs) and for understanding how extracellular electric fields and transcranial current stimulation affect neuronal activity. It has not yet been established whether or not the permittivity of brain tissue is negligible with regard to neural activity in the frequency range 1 Hz–1 kHz. It has been reported that the permittivity of biological tissue exhibits a strong frequency dependence, referred to as dielectric dispersion [1–7]. Schwan measured the dielectric constant of various types of biological tissue over a wide range of frequencies and identified three major dispersion regions: α dispersion (10^5 – 10^6 in the range 10 Hz–1 kHz), β dispersion (10^2 – 10^5 in the range 1 kHz–1 MHz), and γ dispersion (below 10^2 in the GHz range). Taking these observations into account, it has been argued that the capacitive effects of biological tissue in the 1 Hz to several kHz range are negligible [8] and that a macroscopic mass of tissue subjected to an oscillating electric field in this range behaves as a purely resistive material. In line with this argument, Logothetis *et al.* measured the impedance spectrum in cortical tissue of the brain of a monkey *in vivo* and reported that the amplitude

of the impedance drops by only 1.9 dB as the frequency increases from 1 Hz to 5 kHz. They concluded that cortical tissue possesses the properties of a simple ohmic conductor [9]. However, Gabriel *et al.* reported higher values of the permittivity in brain tissues: 10^7 – 10^8 in the 10–100 Hz frequency range [10–12]. If this actually is correct, it may not be valid to consider brain tissue as an ohmic conductor. However, there is yet no theory that accounts for such unusually high permittivity in the low-frequency range [13,14]. The Maxwell-Wagner-Sillars theory describes β dispersion, but the dielectric increment predicted by this theory is far too small to account for the large permittivity at low frequency. Counterion polarization theories describe α dispersion, but in the case of long neurites these theories only account for the dispersion at frequencies lower than 1 Hz [15]. In order to determine whether we can safely ignore capacitive properties of brain tissue and other types of biological tissue, we need to better understand the mechanisms of low-frequency dielectric dispersion.

Recently, we reported theoretically that a significant amount of secondary current flows axially along a cable when it is subjected to a direct-current (dc) electric field [16]. This study was carried out in an attempt to account for the response of the membrane potential of hippocampal pyramidal neurons to a dc electric field [17,18]. Recent experimental and numerical studies suggested that the membrane resistivity of the distal apical dendrites of cortical and hippocampal pyramidal neurons may be significantly lower than that of the proximal dendrites and the soma [19–22]. In the previous work, the inhomogeneous membrane resistivity of dendrites

*Present address: Department of Computational Intelligence and System Science, Tokyo Institute of Technology, 4259 Nagatsuta, Midori-ku, Kanagawa, Japan; aonishi@dis.titech.ac.jp

was modeled by assuming that its effect can be approximated by the effect of the shunt conductance attached to the uniform cable at one end, and we analytically solved cable equations for finite cylindrical cables with and without a leak conductance attached to one end. Then, we showed that spread speeds of the secondary longitudinal current in a cable with a shunt conductance attached to one end are slower than those in a cable with both ends sealed (see Fig. 6 in Ref. [16]). Here, we conjecture that the abundance of electrically long neurites, i.e., dendrites and axons, might cause the low-frequency dielectric dispersion of brain tissue, noting that the secondary longitudinal current in the neurites might provide the slow polarization necessary to yield low-frequency dispersion. To test this idea, here we analytically calculate the membrane potential and the extracellular potential of a passive cable in cases with and without a shunt conductance attached to one end, in the presence of an alternating-current (ac) electric field. First, we model brain tissue as a purely resistive extracellular medium and multiple cables aligned in the same direction, and under assumptions of symmetry described below, we prove that the tissue model packed with multiple cables is equivalent to an isolated system consisting of a single cable and a surrounding extracellular resistive medium. Thus, under the symmetry assumptions, the electrical behavior of the tissue can be described with a set of equations for the membrane potential and the extracellular potential of such a single cable. To solve the equation for the ac electrical field, we use the Green's function we obtained in a previous study [16]. By choosing physiologically reasonable values for the diameter, length, and the capacitance of the membrane, the resistivity of the membrane, the intracellular space, and the extracellular space, we calculate the membrane potential and the extracellular potential for the ac field with the frequency in the range 1 Hz–1 MHz. Then, from the extracellular potential, we calculate the effective permittivity and the conductance of the tissue.

Our calculation shows that the effective permittivity of the tissue for the direction parallel to the cable can be greater than 10^8 at low frequency if the cable is sufficiently long, but the tissue does not possess low-pass filtering characteristics. We conjecture that a very large effective permittivity of brain tissue in the low-frequency region may result from the existence of long, cablelike structures, and the magnitude of the capacitive current in the tissue may be comparable to the magnitude of the resistive current even in the low-frequency region. Moreover, we obtain results suggesting that extremely large permittivity and capacitive current in the low-frequency region can coexist with weak low-pass filter characteristics in the tissue.

II. METHOD

A. Mean field model of brain tissue consisting of N identical passive cables and a purely resistive extracellular medium

Brain tissue is dense with elongated neurites aligned in the same direction, as shown in Fig. 1(A). In this paper, we aim to analytically describe the electric response of an extracellular medium to extracellular stimuli created by an anode and a cathode placed in the extracellular space [Fig. 1(A)]. Brain tissue subjected to an electric field is described by a model consisting of N cables and a three-dimensional extracellular space filled with a purely resistive medium. For the purpose of

mathematical tractability and simplicity, we assume that all of the N cables are identical and aligned in the same direction, the extracellular resistive medium is spatially uniform, and the currents in the intracellular and the extracellular spaces flow longitudinally and are uniformly distributed over the cross sections of the respective structures. Under these symmetry assumptions, the three-dimensional extracellular resistive extracellular space can be described by a single one-dimensional resistive extracellular space and the tissue can be described by a mean field model in which the N identical cables are mutually coupled only through the one-dimensional resistive extracellular space as shown in Fig. 1(B) [23].

Brain tissue subjected to an electric field is described by a model consisting of N cables and a three-dimensional extracellular space filled with a purely resistive medium. For the purpose of mathematical tractability and simplicity, we assume that all of the N cables are identical and aligned in the same direction, the extracellular resistive medium is spatially uniform, and the currents in the intracellular and the extracellular spaces flow longitudinally and are uniformly distributed over the cross sections of the respective structures. Under these symmetry assumptions, the three-dimensional extracellular resistive extracellular space can be described by a single one-dimensional resistive extracellular space and the tissue can be described by a mean field model in which the N identical cables are mutually coupled only through the one-dimensional resistive extracellular space as shown in Fig. 1(B) [23].

In the circuit illustrated in Fig. 1(B), Kirchhoff's first law yields the following equations for the intracellular potential $V_{\text{in}}^k(x, t)$ of the cable k ($=1, 2, \dots, N$), and the extracellular potential $V_{\text{ext}}(x, t)$:

$$\frac{1}{r_{\text{in}}} \sum_{k=1}^N \frac{\partial^2 V_{\text{in}}^k(x, t)}{\partial x^2} = -\frac{1}{\tilde{r}_{\text{ext}}} \frac{\partial^2 V_{\text{ext}}(x, t)}{\partial x^2}, \quad (1)$$

$$\begin{aligned} \frac{1}{r_{\text{in}}} \frac{\partial^2 V_{\text{in}}^k(x, t)}{\partial x^2} &= c_{\text{mem}} \frac{\partial [V_{\text{in}}^k(x, t) - V_{\text{ext}}(x, t)]}{\partial t} \\ &+ \frac{1}{r_{\text{mem}}} [V_{\text{in}}^k(x, t) - V_{\text{ext}}(x, t)]. \end{aligned} \quad (2)$$

Here, r_{in} and \tilde{r}_{ext} are the intracellular resistance (Ω/cm) of each identical cable and extracellular resistance (Ω/cm), and r_{mem} and c_{mem} are the membrane resistance ($\Omega \text{ cm}$) and membrane capacitance (F/cm) of each identical cable.

Because identical cables do not interact directly between each other but only through the single one-dimensional resistive extracellular space, N identical cables have the same membrane potential as each other:

$$V_{\text{in}}^k(x, t) = V_{\text{in}}(x, t). \quad (3)$$

In this condition, defining $V_{\text{mem}}(x, t)$ as $V_{\text{in}}(x, t) - V_{\text{ext}}(x, t)$, Eqs. (1) and (2) can be rewritten as

$$r_{\text{mem}} c_{\text{mem}} \frac{\partial V_{\text{mem}}(x, t)}{\partial t} = \frac{r_{\text{mem}}}{r_{\text{in}} + N\tilde{r}_{\text{ext}}} \frac{\partial^2 V_{\text{mem}}(x, t)}{\partial x^2} - V_{\text{mem}}(x, t), \quad (4)$$

$$\frac{r_{\text{mem}}}{\tilde{r}_{\text{ext}}} \frac{\partial^2 V_{\text{ext}}(x, t)}{\partial x^2} = -\frac{r_{\text{mem}}}{r_{\text{in}} + N\tilde{r}_{\text{ext}}} \frac{\partial^2 V_{\text{mem}}(x, t)}{\partial x^2}. \quad (5)$$

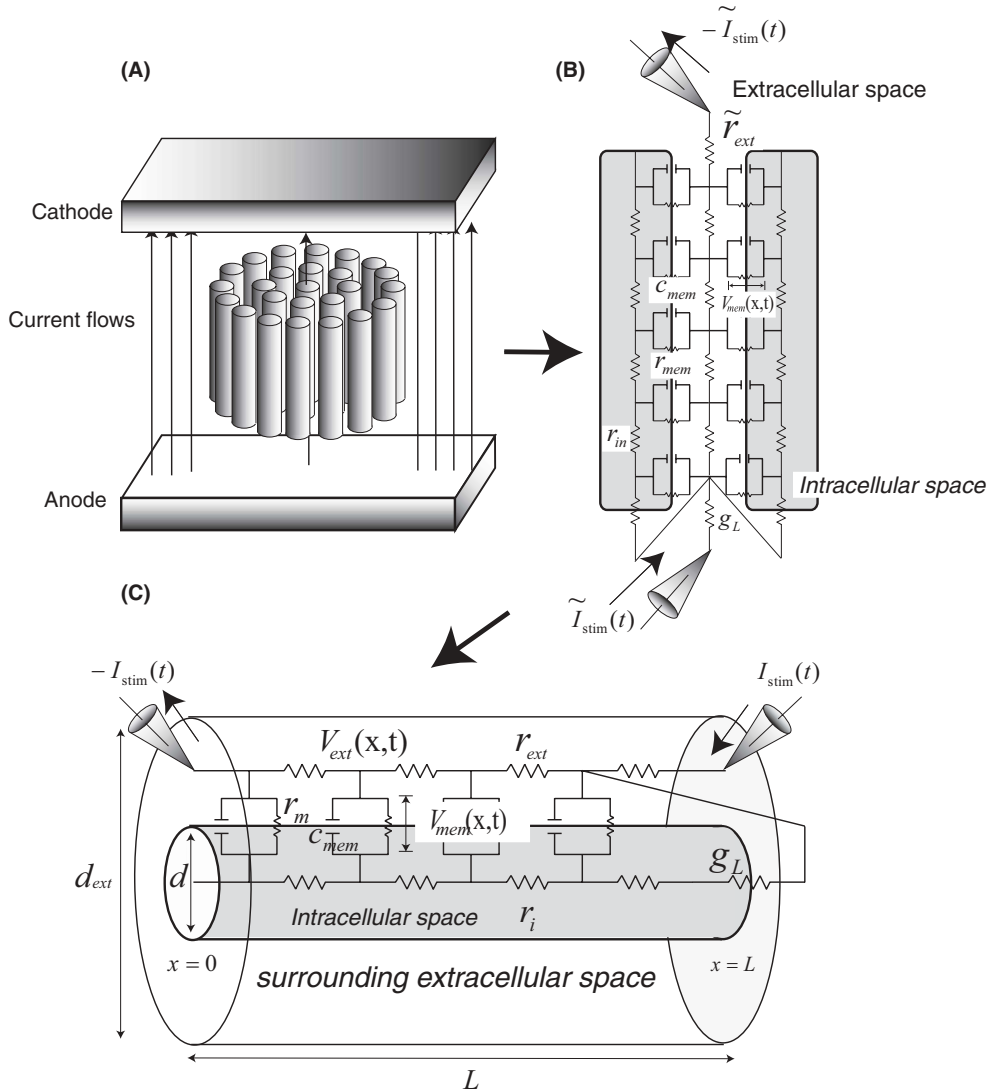


FIG. 1. A model of brain tissue dense with neurites. (A) Brain tissue is densely packed with neurites elongated along the same direction. To model the dielectric properties of brain tissue, we derive an analytical description of the electric response of the extracellular medium to extracellular stimuli created by an anode and a cathode situated in the extracellular space. Brain tissue subjected to an electric field is described by a model consisting of N cables and an extracellular space filled with a purely resistive medium. (B) Mean field model consisting of N identical cables mutually coupled only through a single one-dimensional resistive extracellular space. Under the assumption that all of the N cables are identical and aligned in the same direction, the extracellular resistive medium is spatially uniform, and the currents in the intracellular and the extracellular spaces flow longitudinally and are uniformly distributed over the cross sections of the respective structures, the tissue packed with multiple identical cables can be exactly described by the mean field model. (C) Equivalent single cable model. Under the symmetry assumptions described above, the mean field model is equivalent to an isolated system consisting of a single cable and a surrounding extracellular resistive medium. The extracellular region is assumed to occupy the region between two coaxial cylinders of diameters d and d_{ext} ($d_{ext} > d$), while the intercellular region (i.e., the cable) occupies the region inside the inner cylinder.

Thus, the mean field model is equivalent to a single cable model. Note that Eq. (5) has the same form as the Poisson equation, which is often used in current source density (CSD) analysis.

B. Boundary conditions

We consider N identical cables of length of L (cm) subjected to an ac electric field created by an anode and cathode located in the extracellular space [16,24], as shown

in Fig. 1(A). Stuart and Spruston [19], Inoue *et al.* [20], Golding *et al.* [21], Omori *et al.* [22], and Akiyama *et al.* [18] reported that the membrane resistivity of the distal apical dendrites of cortical and hippocampal pyramidal neurons may be significantly lower than that of the proximal dendrites and the soma. As in a previous work [16], the inhomogeneous membrane resistance of dendrites is modeled by assuming that its effect can be approximated by the effect of the shunt conductance g_L attached to the uniform cable at $x = L$. In the mean field model, this situation is characterized by

the following boundary conditions, which are straightforward extensions of those used in Monai *et al.* [16]:

$$\begin{aligned} \left. \frac{\partial V_{\text{in}}^k(x,t)}{\partial x} \right|_{x=0} &= 0, \\ \left. \frac{\partial V_{\text{in}}^k(x,t)}{\partial x} \right|_{x=L} &= -r_{\text{in}} g_L [V_{\text{in}}^k(L,t) - V_{\text{ext}}(L,t)], \quad (6) \\ (k &= 1, \dots, N), \end{aligned}$$

$$\begin{aligned} \left. \frac{\partial V_{\text{ext}}(x,t)}{\partial x} \right|_{x=0} &= -\tilde{r}_{\text{ext}} \tilde{I}_{\text{stim}}(t), \\ \left. \frac{\partial V_{\text{ext}}(x,t)}{\partial x} \right|_{x=L} &= -\tilde{r}_{\text{ext}} \tilde{I}_{\text{stim}}(t) \\ &+ \tilde{r}_{\text{ext}} \sum_{k=1}^N g_L [V_{\text{in}}^k(L,t) - V_{\text{ext}}(L,t)]. \quad (7) \end{aligned}$$

Here, $\tilde{I}_{\text{stim}}(t)$ is a time-varying stimulus current created by the anode and cathode located in the extracellular space. If $g_L = 0$, then the cable is sealed at both ends and symmetric with respect to direction along its axis. In this case, there is no current flow through either end. If $g_L \neq 0$, then at $x = L$, some current flows between the intracellular and the extracellular media through the shunt. As mentioned above, in the mean field model, N identical cables have the same membrane potential as each other. Applying Eq. (3) to those boundary conditions and subtracting the boundary conditions for the intracellular potential from those for the extracellular potential, we derive the boundary conditions for the membrane potential:

$$\begin{aligned} \left. \frac{\partial V_{\text{mem}}(x,t)}{\partial x} \right|_{x=0} &= \tilde{r}_{\text{ext}} \tilde{I}_{\text{stim}}(t), \\ \left. \frac{\partial V_{\text{mem}}(x,t)}{\partial x} \right|_{x=L} &= \tilde{r}_{\text{ext}} \tilde{I}_{\text{stim}}(t) - (r_{\text{in}} + N\tilde{r}_{\text{ext}}) g_L V_{\text{mem}}(L,t). \quad (8) \end{aligned}$$

Using the definition of the membrane potential, we can rewrite the boundary conditions for the extracellular potential as

$$\begin{aligned} \left. \frac{\partial V_{\text{ext}}(x,t)}{\partial x} \right|_{x=0} &= -\tilde{r}_{\text{ext}} \tilde{I}_{\text{stim}}(t), \\ \left. \frac{\partial V_{\text{ext}}(x,t)}{\partial x} \right|_{x=L} &= -\tilde{r}_{\text{ext}} \tilde{I}_{\text{stim}}(t) + N\tilde{r}_{\text{ext}} g_L V_{\text{mem}}(L,t). \quad (9) \end{aligned}$$

Generally, it is difficult to solve differential equations with such time-varying boundary conditions. To avoid this difficulty, we consider a physically equivalent system in which the complicating time dependence of the boundary conditions is removed and the same effect is accounted for through the introduction of the following current density existing in both the intercellular and extracellular media:

$$\tilde{I}_{\text{cd}}(x,t) = \tilde{I}_{\text{stim}}(t) [\delta(x - \Delta x) - \delta(x - L + \Delta x)]. \quad (10)$$

Here, $\delta(t)$ is the Dirac δ function and Δx is an infinitesimal distance along the cable. A detailed description of this mathematical manipulation is given in our previous paper [16]. The leak current through the shunt conductance at $x = L$ represented in the extracellular boundary conditions [Eq. (9)] is also replaced by a current density given along the extracellular medium as $\delta(x - L + \Delta x) g_L V_{\text{mem}}(L,t)$. With these mathematical manipulations, Eqs. (3) and (4) are now

replaced with the following equations for the membrane potential and the extracellular potential:

$$\begin{aligned} r_{\text{mem}} c_{\text{mem}} \frac{\partial V_{\text{mem}}(x,t)}{\partial t} &= \frac{r_{\text{mem}}}{r_{\text{in}} + N\tilde{r}_{\text{ext}}} \frac{\partial^2 V_{\text{mem}}(x,t)}{\partial x^2} - V_{\text{mem}}(x,t) \\ &- \frac{r_{\text{mem}}}{r_{\text{in}} + N\tilde{r}_{\text{ext}}} \tilde{r}_{\text{ext}} \tilde{I}_{\text{cd}}(x,t), \quad (11) \end{aligned}$$

$$\begin{aligned} \frac{r_{\text{mem}}}{\tilde{r}_{\text{ext}}} \frac{\partial^2 V_{\text{ext}}(x,t)}{\partial x^2} &= -\frac{r_{\text{mem}}}{r_{\text{in}} + N\tilde{r}_{\text{ext}}} \frac{\partial^2 V_{\text{mem}}(x,t)}{\partial x^2} \\ &- \delta(x - L) r_{\text{mem}} g_L V_{\text{mem}}(L,t) \\ &- \frac{r_{\text{mem}}}{r_{\text{in}} + N\tilde{r}_{\text{ext}}} r_{\text{in}} \tilde{I}_{\text{cd}}(x,t). \quad (12) \end{aligned}$$

For this system, the boundary conditions are

$$\left. \frac{\partial V_{\text{mem}}(x,t)}{\partial x} \right|_{x=0} = 0, \quad (13)$$

$$\left. \frac{\partial V_{\text{mem}}(x,t)}{\partial x} \right|_{x=L} = -(r_{\text{in}} + N\tilde{r}_{\text{ext}}) g_L V_{\text{mem}}(L,t),$$

$$\left. \frac{\partial V_{\text{ext}}(x,t)}{\partial x} \right|_{x=0} = 0, \quad \left. \frac{\partial V_{\text{ext}}(x,t)}{\partial x} \right|_{x=L} = 0. \quad (14)$$

Equation (13) specifies a reflecting boundary condition at $x = 0$ and a leaky boundary condition at $x = L$, while Eq. (14) specifies reflecting boundary conditions at both ends.

C. An equivalent single cable model

Replacing $N\tilde{r}_{\text{ext}}$, $\tilde{I}_{\text{stim}}(t)/N$ and $\tilde{I}_{\text{cd}}(x,t)/N$ with r_{ext} , $I_{\text{stim}}(t)$ and $I_{\text{cd}}(x,t)$ respectively, a system described by Eqs. (11)–(14) becomes equivalent to a single cable model with a shunt conductance attached to one end [Fig. 1(C)] [16]. From Eq. (10), the newly introduced current density $I_{\text{cd}}(x,t)$ becomes $I_{\text{cd}}(x,t) = I_{\text{stim}}(t) [\delta(x - \Delta x) - \delta(x - L + \Delta x)]$. $N\tilde{r}_{\text{ext}}$ can be mathematically interpreted as the resistivity of one of N extracellular subspaces into which the extracellular space of the mean field model is equally divided, and $\tilde{I}_{\text{stim}}(t)/N$ can be interpreted as the value of the stimulus current flowing through one of the N extracellular subspaces. Therefore, under the symmetric assumptions described above, the tissue packed with multiple cables can be exactly described by an isolated system consisting of a single cable and a surrounding extracellular resistive medium, which is given by

$$\begin{aligned} \tau_{\text{mem}} \frac{\partial V_{\text{mem}}(x,t)}{\partial t} &= \lambda_{\text{mem}}^2 \frac{\partial^2 V_{\text{mem}}(x,t)}{\partial x^2} - V_{\text{mem}}(x,t) \\ &- \lambda_{\text{mem}}^2 r_{\text{ext}} I_{\text{cd}}(x,t), \quad (15) \end{aligned}$$

$$\begin{aligned} \frac{r_{\text{mem}}}{r_{\text{ext}}} \frac{\partial^2 V_{\text{ext}}(x,t)}{\partial x^2} &= -\lambda_{\text{mem}}^2 \frac{\partial^2 V_{\text{mem}}(x,t)}{\partial x^2} - \delta(x - L) r_{\text{mem}} g_L \\ &\times V_{\text{mem}}(L,t) - \lambda_{\text{mem}}^2 r_{\text{in}} I_{\text{cd}}(x,t), \quad (16) \end{aligned}$$

where λ_{mem} and τ_{mem} are the space constant (cm) and time constant (msec), defined by

$$\lambda_{\text{mem}} = \sqrt{\frac{r_{\text{mem}}}{r_{\text{in}} + r_{\text{ext}}}} \quad \text{and} \quad \tau_{\text{mem}} = r_{\text{mem}} c_{\text{mem}}.$$

For this system, the boundary conditions are

$$\left. \frac{\partial V_{\text{mem}}(x,t)}{\partial x} \right|_{x=0} = 0, \quad (17)$$

$$\left. \frac{\partial V_{\text{mem}}(x,t)}{\partial x} \right|_{x=L} = -(r_{\text{in}} + r_{\text{ext}})g_L V_{\text{mem}}(L,t),$$

$$\left. \frac{\partial V_{\text{ext}}(x,t)}{\partial x} \right|_{x=0} = 0, \quad \left. \frac{\partial V_{\text{ext}}(x,t)}{\partial x} \right|_{x=L} = 0. \quad (18)$$

In order to define the intracellular resistivity r_{int} and the extracellular resistivity r_{ext} , the extracellular region is assumed to occupy the region between two coaxial cylinders of diameters d and d_{ext} ($d_{\text{ext}} > d$), while the intercellular region (i.e., the cable) occupies the region inside the inner cylinder [see Fig. 1(C)]. With the equivalent system represented by Eqs. (15)–(18), we can derive analytic solution for any wave form of stimulus current $I_{\text{stim}}(t)$. This is demonstrated in the following.

D. Derivation of analytical solution

1. Membrane potential

Equation (15) is equivalent to the cable equation used in Monai *et al.* [16], from which the membrane potential can be calculated independently of the extracellular potential, and thus the theory developed there can be applied to this equation. In this way, we obtain the following analytic solution of the membrane potential in response to the extracellular stimulus $I_{\text{stim}}(t)$:

$$V_{\text{mem}}(x,t) = \frac{r_{\text{ext}}\lambda_{\text{mem}}^2}{\tau_{\text{mem}}} \sum_{n=0}^{\infty} \frac{\varphi_n(L) - \varphi_n(0)}{\alpha_n} \varphi_n(x) \times \int_0^t dt' \exp\left(-\frac{t-t'}{\kappa_n}\right) I_{\text{stim}}(t'), \quad (19)$$

$$\alpha_n = \frac{L}{2} + \frac{r_{\text{in}}g_L}{2} \left(\frac{\varphi_n(L)}{\mu_n}\right)^2. \quad (20)$$

The set of eigenvalues $\{\mu_n\}$ and eigenfunctions $\{\varphi_n(x)\}$ which satisfy the boundary conditions appearing in Eq. (17) are given by the expressions [16,25–28]

$$\mu_n \tan(\mu_n L) = (r_{\text{in}} + r_{\text{ext}})g_L; \quad n = 0, 1, 2, \dots, \quad (21)$$

$$\varphi_n(x) = \cos(\mu_n x), \quad (22)$$

where the eigenvalues μ_n obey the transcendental equation [Eq. (21)]. The time constants κ_n are given by

$$\kappa_n = \frac{\tau_{\text{mem}}}{1 + \mu_n^2 \lambda_{\text{mem}}^2} \quad (\text{msec}). \quad (23)$$

When $g_L = 0$ (sealed-end case), the eigenvalues and eigenfunctions given in Eqs. (21) and (22) become

$$\mu_n = \frac{n\pi}{L}, \quad \varphi_n(x) = \cos\left(\frac{n\pi}{L}x\right).$$

2. Extracellular potential

Here, we derive an analytic solution representing the extracellular potential in response to the extracellular stimulus

created by the anode and cathode. A detailed description of the derivation is given in the Appendix.

Generally, the extracellular potential in the cable model, depicted in Fig. 1(B), is indefinite, because there is no explicit definition of the ground to uniquely determine its value. However, there is a special case: If stimuli induced by an anode and a cathode, either the anode or the cathode can be regarded as the ground electrode because the sum of the stimulus currents entering and exiting the circuit is zero. Thus, in this case, the extracellular potential can be defined.

As mentioned above, the membrane potential can be calculated independently of the extracellular potential. Therefore, the right-hand side term of Eq. (16), which consists of the membrane potential and the stimulus current $I_{\text{stim}}(t)$, can be regarded as the current density determined independently along the extracellular medium. By convolving the right-hand side, into which Eq. (19) is substituted, with the Green's function of the Poisson equation [Eq. (16)], we obtain the analytic solution of the extracellular potential:

$$V_{\text{ext}}(x,t) = -\frac{I_{\text{stim}}(t)}{2} \frac{r_{\text{in}}r_{\text{ext}}}{r_{\text{in}} + r_{\text{ext}}} (2x - L) - \frac{r_{\text{ext}}}{r_{\text{in}} + r_{\text{ext}}} V_{\text{mem}}(x,t) + g_L \frac{r_{\text{ext}}^2 \lambda_{\text{mem}}^2}{\tau_{\text{mem}}} \sum_{n=0}^{\infty} \frac{1}{\mu_n^2} \frac{\varphi_n(L) - \varphi_n(0)}{\alpha_n} \varphi_n(L) \times \int_0^t dt' \exp\left(-\frac{t-t'}{\kappa_n}\right) I_{\text{stim}}(t'). \quad (24)$$

When $g_L = 0$ (sealed-end case), this analytic solution takes the simple form

$$V_{\text{ext}}(x,t) = -\frac{I_{\text{stim}}(t)}{2} \frac{r_{\text{in}}r_{\text{ext}}}{r_{\text{in}} + r_{\text{ext}}} (2x - L) - \frac{r_{\text{ext}}}{r_{\text{in}} + r_{\text{ext}}} V_{\text{mem}}(x,t). \quad (25)$$

E. Model parameters and numerical calculation method

In this paper, to model the low-frequency dielectric dispersion of brain tissue, we focus on the case in which there is a large amount of secondary current flowing axially along the cable when it is exposed to electric field [16]. That there can exist a large amount of secondary current was discovered in studies that attempted to account for the observed responses of the membrane potential of hippocampal CA1 pyramidal neurons subjected to a dc field [17,18]. To realize a consistency with those works, we use the parameter values previously reported for the hippocampal CA1 pyramidal neuron: a specific membrane capacitance of $C_{\text{mem}} = 1.5$ ($\mu\text{F}/\text{cm}^2$) [20], a specific membrane resistivity of $R_{\text{mem}} = 30$ ($\text{k}\Omega\text{cm}^2$) [20,29,30], and a specific intracellular resistivity of $R_{\text{in}} = 200$ (Ωcm) [30,31]. Also, the diameter of the cable is $d = 1.2$ (μm) [31], and the length of the cable is $L = 700$ (μm) [31], except in the case considered in Fig. 5. In cases depicted in Figs. 2–4, we used a shunt conductance of $g_L = 880$ (pS), as in our previous paper [16]. As mentioned above, the extracellular space is assumed to be a cylinder filled with a purely resistive medium. The diameter of the extracellular space was set to $d_{\text{ext}} = 1.2 \times d$ (μm) (Figs. 2–5), except in the case of Fig. 6. The specific extracellular resistance was set to $R_{\text{ext}} = 100$ (Ωcm). The parameter values used for determining the electric characteristics per unit length of the

cable and the extracellular media were calculated according to the following:

$$r_{\text{mem}} = \frac{R_{\text{mem}}}{\pi d}, \quad r_{\text{in}} = \frac{R_{\text{in}}}{\pi \left(\frac{d}{2}\right)^2},$$

$$r_{\text{ext}} = \frac{R_{\text{ext}}}{\pi \left(\left(\frac{d_{\text{ext}}}{2}\right)^2 - \left(\frac{d}{2}\right)^2\right)}, \quad \text{and} \quad c_{\text{mem}} = C_{\text{mem}} \pi d.$$

It is impossible to numerically solve Eqs. (15) and (16) under the boundary conditions [Eqs. (17) and (18)], due to the indefiniteness inherent in solving the Poisson equation [Eq. (16)] under the reflecting boundary condition. Instead, employing an implicit method, we numerically solved an extended model consisting of a passive cable and an extracellular medium connected to a ground with very small conductance (see Fig. 8). We found that the numerical computations give values that are close to the analytic solution obtained in this paper (see Fig. 9). A detailed explanation of the extended model is given in the Appendix.

The analytic solution derived here has the form of a Fourier series expansion in the eigenfunctions $\{\phi_n(x)\}$ and $\{\cos(n\pi x/L)\}$, as shown in Eqs. (19), (24), and (25). This Fourier series must be calculated numerically. The infinite series contained in these equations were truncated at $n = 1000$, and the eigenvalues μ_n , satisfying Eq. (21), were calculated with this truncated Newton's method [32]. In the shunt-end case, the deviation of the results obtained from this truncated Fourier series from those obtained in the numerical simulations is 0.382% at the steady state when applying a dc stimulus.

III. RESULTS

A. Response to dc extracellular stimulus

First, we consider the case of a dc step current stimulus, $I_{\text{stim}}(t) = I_0 \times u(t)$, where I_0 is the amplitude of the dc step current and $u(t)$ is a dc step current defined as follows:

$$u(t) = \begin{cases} 1 & (t \geq 0), \\ 0 & (t < 0). \end{cases}$$

From Eqs. (19) and (24), we find that the membrane potential and the extracellular potential in response to the dc step stimulus are

$$V_{\text{mem}}(x,t) = I_0 \frac{r_{\text{ext}} \lambda_{\text{mem}}^2}{\tau_{\text{mem}}} \sum_{n=0}^{\infty} \frac{\varphi_n(L) - \varphi_n(0)}{\alpha_n} \varphi_n(x) \kappa_n \times \left[1 - \exp\left(-\frac{t}{\kappa_n}\right) \right], \quad (26)$$

$$V_{\text{ext}}(x,t) = -\frac{I_0 u(t)}{2} \frac{r_{\text{in}} r_{\text{ext}}}{r_{\text{in}} + r_{\text{ext}}} (2x - L) - \frac{r_{\text{ext}}}{r_{\text{in}} + r_{\text{ext}}} V_{\text{mem}}(x,t) + I_0 g_L \frac{r_{\text{ext}}^2 \lambda_{\text{mem}}^2}{\tau_{\text{mem}}} \sum_{n=0}^{\infty} \frac{1}{\mu_n^2} \frac{\varphi_n(L) - \varphi_n(0)}{\alpha_n} \varphi_n(L) \kappa_n \times \left[1 - \exp\left(-\frac{t}{\kappa_n}\right) \right]. \quad (27)$$

When $g_L = 0$ (sealed-end case), these solutions take the simple forms

$$V_{\text{mem}}(x,t) = I_0 \frac{r_{\text{ext}} \lambda_{\text{mem}}^2}{\tau_{\text{mem}}} \sum_{n=0}^{\infty} \frac{\cos(n\pi) - \cos(0)}{\frac{L}{2}} \times \cos\left(\frac{n\pi}{L} x\right) \kappa_n \left[1 - \exp\left(-\frac{t}{\kappa_n}\right) \right], \quad (28)$$

$$V_{\text{ext}}(x,t) = -\frac{I_0 u(t)}{2} \frac{r_{\text{in}} r_{\text{ext}}}{r_{\text{in}} + r_{\text{ext}}} (2x - L) - \frac{r_{\text{ext}}}{r_{\text{in}} + r_{\text{ext}}} V_{\text{mem}}(x,t). \quad (29)$$

Figure 2 plots the time dependence of the membrane potential [Figs. 2(A) and 2(C)] and the extracellular potential [Figs. 2(B) and 2(D)] in response to the dc step stimulus. As seen there, the membrane potential exhibits slow hyperpolarization after rapid depolarization (i.e., a biphasic change) at the shunt end, as previously reported [16–18,22,28], while the extracellular potential changes monotonically at both ends of the cable, even in the shunt-end case.

B. Frequency response

Next, we consider the case of an ac stimulus, $I_{\text{stim}}(t) = I_0 \exp(j\omega t)$, where I_0 is the amplitude of the current and ω is the angular frequency. From Eqs. (19) and (24), we find that the membrane potential and the extracellular potential in response to this ac stimulus are

$$V_{\text{mem}}(x,\omega) = I_0 \frac{r_{\text{ext}} \lambda_{\text{mem}}^2}{\tau_{\text{mem}}} \sum_{n=0}^{\infty} \frac{\varphi_n(L) - \varphi_n(0)}{\alpha_n} \varphi_n(x) \frac{1}{\frac{1}{\kappa_n} + j\omega}, \quad (30)$$

$$V_{\text{ext}}(x,\omega) = -\frac{I_0}{2} \frac{r_{\text{in}} r_{\text{ext}}}{r_{\text{in}} + r_{\text{ext}}} (2x - L) - \frac{r_{\text{ext}}}{r_{\text{in}} + r_{\text{ext}}} V_{\text{mem}}(x,t) + I_0 g_L \frac{r_{\text{ext}}^2 \lambda_{\text{mem}}^2}{\tau_{\text{mem}}} \sum_{n=0}^{\infty} \frac{1}{\mu_n^2} \frac{\varphi_n(L) - \varphi_n(0)}{\alpha_n} \times \varphi_n(L) \frac{1}{\frac{1}{\kappa_n} + j\omega}. \quad (31)$$

When $g_L = 0$ (sealed-end case), we have

$$V_{\text{mem}}(x,\omega) = I_0 \frac{r_{\text{ext}} \lambda_{\text{mem}}^2}{\tau_{\text{mem}}} \sum_{n=0}^{\infty} \frac{\cos(n\pi) - \cos(0)}{\frac{L}{2}} \times \cos\left(\frac{n\pi}{L} x\right) \frac{1}{\frac{1}{\kappa_n} + j\omega} = \frac{r_{\text{ext}}}{2} \frac{I_0 \lambda_{\text{mem}}}{j\omega \sqrt{1 + j\omega \tau_{\text{mem}}}} \frac{\sinh\left(\frac{\sqrt{1 + j\omega \tau_{\text{mem}}}}{\lambda_{\text{mem}}} \frac{2x - L}{2}\right)}{\cosh\left(\frac{\sqrt{1 + j\omega \tau_{\text{mem}}}}{\lambda_{\text{mem}}} \frac{L}{2}\right)}, \quad (32)$$

$$V_{\text{ext}}(x,\omega) = -\frac{I_0}{2} \frac{r_{\text{in}} r_{\text{ext}}}{r_{\text{in}} + r_{\text{ext}}} (2x - L) - \frac{r_{\text{ext}}}{r_{\text{in}} + r_{\text{ext}}} V_{\text{mem}}(x,\omega). \quad (33)$$

Note that the frequency response of the membrane potential can be rewritten in terms of hyperbolic functions, as reported previously [16,24,33].

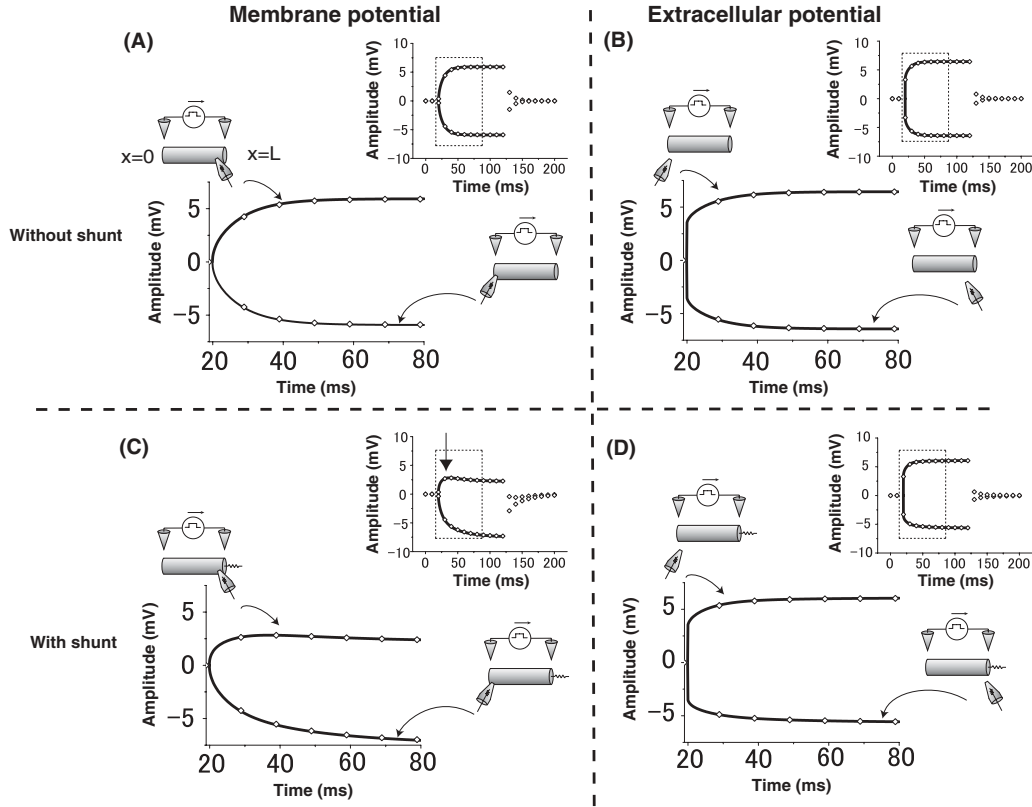


FIG. 2. Response to direct-current (dc) extracellular stimulus. (A), (C) The membrane potential in response to a dc stimulus in the cases $g_L = 0$ [pS] (without a shunt) and $g_L = 880$ (pS) (with a shunt). (B), (D) The extracellular potential in response to a dc stimulus in the cases $g_L = 0$ (pS) (without a shunt) and $g_L = 880$ (pS) (with a shunt). In each panel, the solid curves represent the analytical solutions. The dc stimulus is applied from 20 (msec) to 120 (msec) in the case depicted in the inset and from 20 (msec) to 80 (msec) in another case. The open diamonds denote the numerical solutions of the cable equations. The resistor sticking out of the cable at the $x = L$ end represents the shunt conductance g_L , and the cone with a resistor inside it represents a recording electrode. The diameter of the cable is $d = 1.2$ (μm), and the diameter of the extracellular space is $d_{\text{ext}} = 1.2d$.

Figures 3(A) and 3(B) display the amplitude-frequency response and Figs. 3(C) and 3(D) display the phase-frequency response. As reported previously [16], only the membrane potential at the shunt end ($x = L$) of the cable in the $g_L \neq 0$ case exhibits a frequency preference, and the phase advances [Figs. 3(A) and 3(C)]. In contrast to the frequency preference of the shunt end, the amplitude response of the membrane potential at the sealed end of the cable with and without the shunt decreases monotonically, approaching zero, and the phase approaches $-\pi/4$ as the frequency of the stimulus increases. Contrastingly, the amplitude of the extracellular potential at both ends of the cables in both cases with and without the shunt drops by only 1.7 dB as the frequency of the stimulus increases from 1 to 400 Hz, and the phase is almost constant as the frequency of the stimulus increases [Figs. 3(B) and 3(D)].

C. Effective permittivity and conductivity

We now calculate the effective conductivity and permittivity, thereby elucidating macroscopic properties of the bulk brain tissue from the frequency responses. The longitudinal extracellular electric field is obtained from the extracellular

potentials at both ends of the cable as

$$E(\omega) = -\frac{V_{\text{ext}}(L, \omega) - V_{\text{ext}}(0, \omega)}{L}. \quad (34)$$

From the definition of the longitudinal extracellular electric field, the effective conductivity $\sigma(\omega)$ and permittivity $\epsilon(\omega)$ of the extracellular medium are related as

$$\sigma(\omega) + j\omega\epsilon(\omega) = \frac{I_0}{E(\omega)}, \quad (35)$$

where I_0 is the amplitude of the ac stimulus current.

Figures 4(A) and 4(B) plot the effective conductivity (S/m) and relative permittivity (\cdot) of the cable in cases without and with the shunt conductance, respectively. As seen there, the relative permittivity in the case with a shunt [Fig. 4(B); $g_L = 880$ (pS)] is slightly larger than that in the case without [Fig. 4(A); $g_L = 0$ (pS)].

Figure 4(C) plots the time constant $\tau(\omega)$ characterizing the dielectric relaxation of the bulk brain tissue, defined by

$$\tau(\omega) = \frac{\epsilon(\omega)}{\sigma(\omega)}. \quad (36)$$

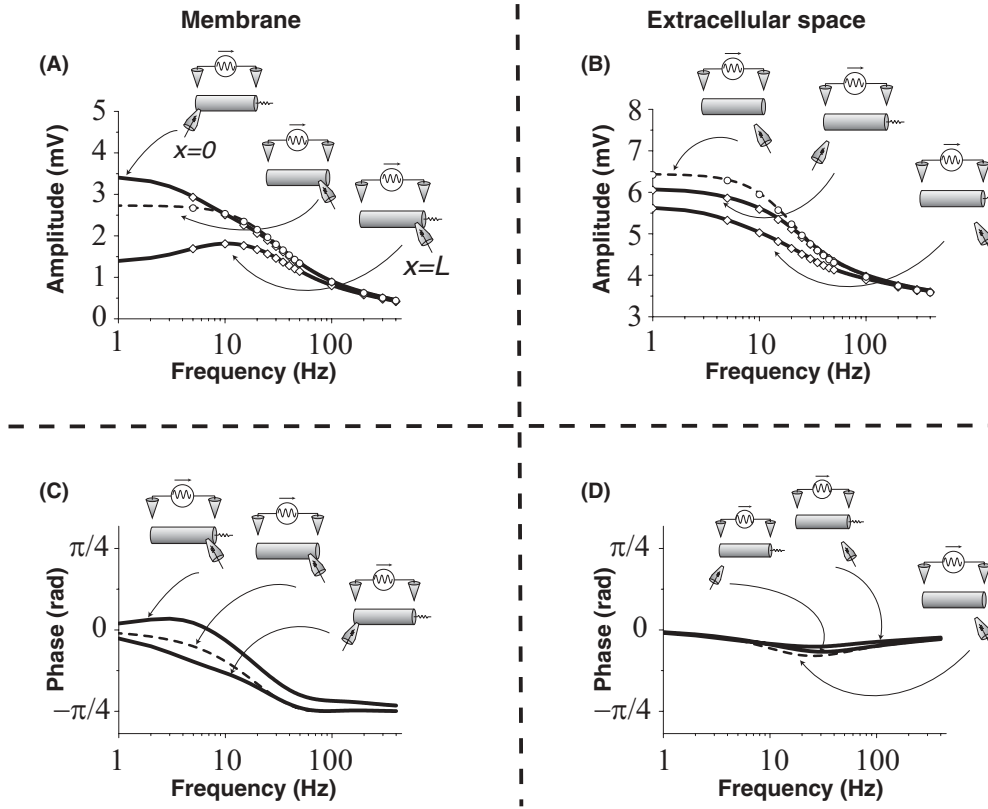


FIG. 3. Weak low-pass filtering characteristics of the extracellular medium. (A), (B) Amplitude-frequency response of the membrane potential and the extracellular potential. (C), (D) Phase-frequency response of the membrane potential and the extracellular potential. The broken and solid curves in each panel represent analytic solutions in the cases $g_L = 0$ (pS) (without a shunt) and $g_L = 880$ (pS) (with a shunt), respectively. The open diamonds denote the numerical solutions of the cable equations. It is seen that the amplitude of extracellular potential drops by only 1.7 dB as frequency increases from 1 to 400 Hz, and the phase of extracellular potential is almost constant over the entire range of frequencies. The diameter of the cable is $d = 1.2$ (μm), and the diameter of the extracellular space is $d_{\text{ext}} = 1.2d$.

The dielectric relaxation time constant in the case with the shunt is approximately 4 (msec), while that in the case without is approximately 3 (msec) in the low-frequency region.

Finally, we calculate the storage factor, defined by

$$\frac{\text{capacitive current}}{\text{resistive current}} = \frac{\omega\epsilon(\omega)}{\sigma(\omega)}. \quad (37)$$

As shown in Figs. 4(A), 4(B), and 4(D), points at which the storage factor is maximized coincide with the corner frequencies of the relative permittivity in both the cases with and without the shunt conductance. The maximum value of the storage factor in the case with a shunt is approximately 0.15, and that in the case without is approximately 0.25 [Fig. 4(d)].

D. Effect of cable length and extracellular space size on low-frequency dielectric dispersion

The results of our calculations for the relative permittivity and the storage factor, using various values of the length of the cable (L) are plotted in Fig. 5(A). As shown in Figs. 5(B) and 5(C), the relative permittivity at 1 Hz increases with the cable length in accordance with a power law, and in Fig. 5(C), the storage factor at low frequency (less than a few Hz) also increases as a function of the cable length. As shown in Figs. 5(B) and 5(C), the corner frequencies of the relative permittivity coincide with the values at which the storage factor

is maximized, which decrease as the cable becomes longer. By contrast, the maximum values of the storage factor are almost constant for any length of the cable.

The results of our calculations for the relative permittivity and the storage factor using various diameters of the extracellular space (d_{ext}) are plotted in Fig. 6(A). As shown in Figs. 6(B) and 6(C), the relative permittivity at 1 Hz decreases with the diameter of the extracellular space in accordance with a power law, and the value at which the storage factor is maximized decreases as the diameter of the extracellular space increases. By contrast, the corner frequencies of the relative permittivity, which coincide with the points at which the storage factor is maximized, are almost constant for any diameter.

IV. DISCUSSION

We have shown theoretically that multiple passive long cables packed in a purely resistive extracellular medium may exhibit a large low-frequency dielectric dispersion by analyzing the equivalent single cable model using the Green's function method. We found that the relative permittivity in the low-frequency range depends strongly on the length of the cable. These results are consistent with our conjecture that the secondary longitudinal current in the cable might

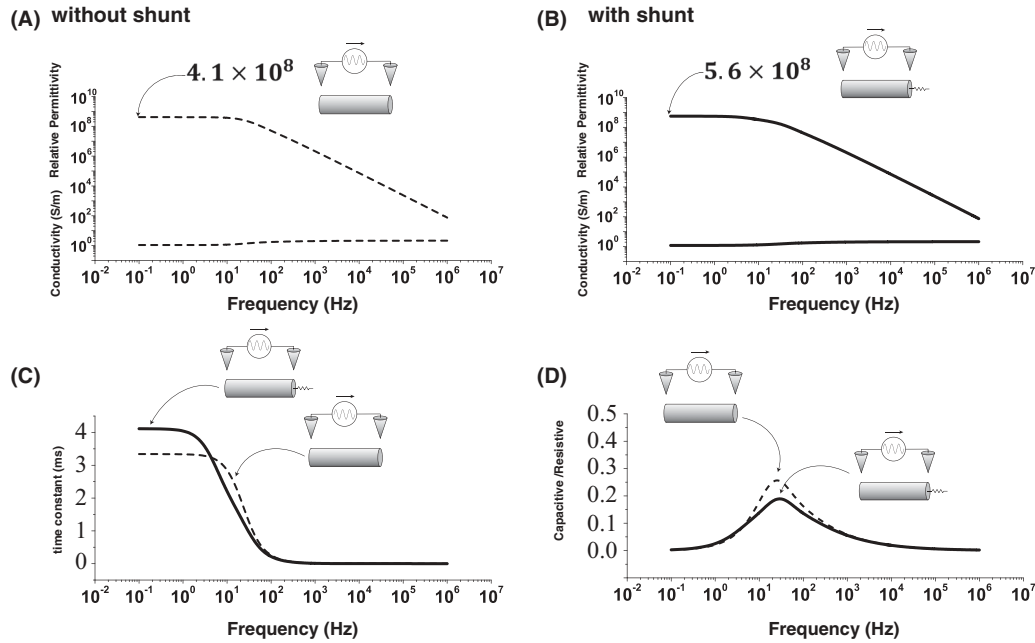


FIG. 4. Extremely large permittivity and capacitive current in the extracellular media. (A) Effective conductivity $\sigma(\omega)$ (S/m) and effective relative permittivity $\epsilon(\omega)$ in the case $g_L = 0$ (pS) (without a shunt). (B) Those in the case of $g_L = 880$ (pS) (with a shunt). (C) Time constant of dielectric relaxation $\tau(\omega)$, defined as $\omega\epsilon(\omega)/\sigma(\omega)$. (D) The storage factor (i.e., the capacitive-to-resistive ratio) defined as $\omega\epsilon(\omega)/\sigma(\omega)$. In each panel, the solid curves and broken curves denote the values in the cases $g_L = 880$ (pS) and $g_L = 0$ (pS), respectively. The extracellular medium has a large relative permittivity of approximately 10^8 in the low-frequency region, and attaching a shunt at one end of the cable only slightly enhances the permittivity. The maximum value of the storage factor is approximately 0.25 when $g_L = 0$ (pS). The diameter of the cable is $d = 1.2$ (μm), and the diameter of the extracellular space is $d_{\text{ext}} = 1.2d$.

cause slow polarization that induces low-frequency dispersion. The results of our theoretical analyses support the hypothesis that brain tissue has a very large effective permittivity in the low-frequency region due to the presence of long neurites and they suggest that the magnitude of the capacitive current in the tissue may be comparable to that of the resistive current in the low-frequency region, despite weak low-pass filtering properties of brain tissue.

A. Effective extracellular space

When one discusses diffusion of chemicals, the term “extracellular space” would be used as a synonym for interstitial space. Many studies reported that the interstitial space in brain tissue is 10–30% of the volume [34–36]. The term “extracellular space,” however, means something different when one discusses the spread of electric current in biological tissues. It is an abstract concept, an imaginary apparent space in which current either generated by cells or provided by external mechanisms flow. The entity of the extracellular space depends on the frequency of the current. In the case of a current with very high frequency, the current can flow across cell membranes as capacitive current. Therefore the extracellular space in this situation would be the entire space including interstitial space, intracellular space, and the membrane. Low-frequency current would not flow across the membrane as capacitive current and the resistive membrane current would be small because of the high resistivity of cell membranes. In this situation, the interstitial space

constitutes the extracellular space [37]. Other than these extreme situations, the extracellular space in electrical sense means an imaginary effective space comprised of the contributions due to the membranes and the intracellular space of nearby cells, including glial cells, in addition to the interstitial space. The electrical properties of the effective space as dielectrics can be described by the effective permittivity and conductance. They are different from those of the interstitial space, intracellular space, and the membrane. In this study, we have shown that the morphology of the cell can be an important factor that determines the effective permittivity and conductivity.

The volume fraction of astroglia cells in the cortical tissue has been reported to be 10–20% (5% in stratum radiatum of rat hippocampal area CA1 [38]) of the neuropile [39,40]. Since the membrane resistivity of the astroglia is lower than that of neurons and astroglia may be connected by gap junctions, glial cells may contribute to the effective permittivity and conductivity partly by constituting the interstitial space and partly by behaving as nearby cables. Considering the volume fraction of average interstitial space and glial cells, we set the extracellular volume fraction as 44% in most of the calculations such as are shown in Figs. 2–5 and Fig. 6(A-b). In Fig. 6(A-a), the volume fraction was set to 10.25%, which is close to the smallest value of the previously reported volume fraction, that of rat hippocampal CA1 region. In both cases, we obtained qualitatively similar results as shown in Fig. 6(B), and a smaller extracellular volume fraction gave rise to more pronounced low-frequency dispersion.

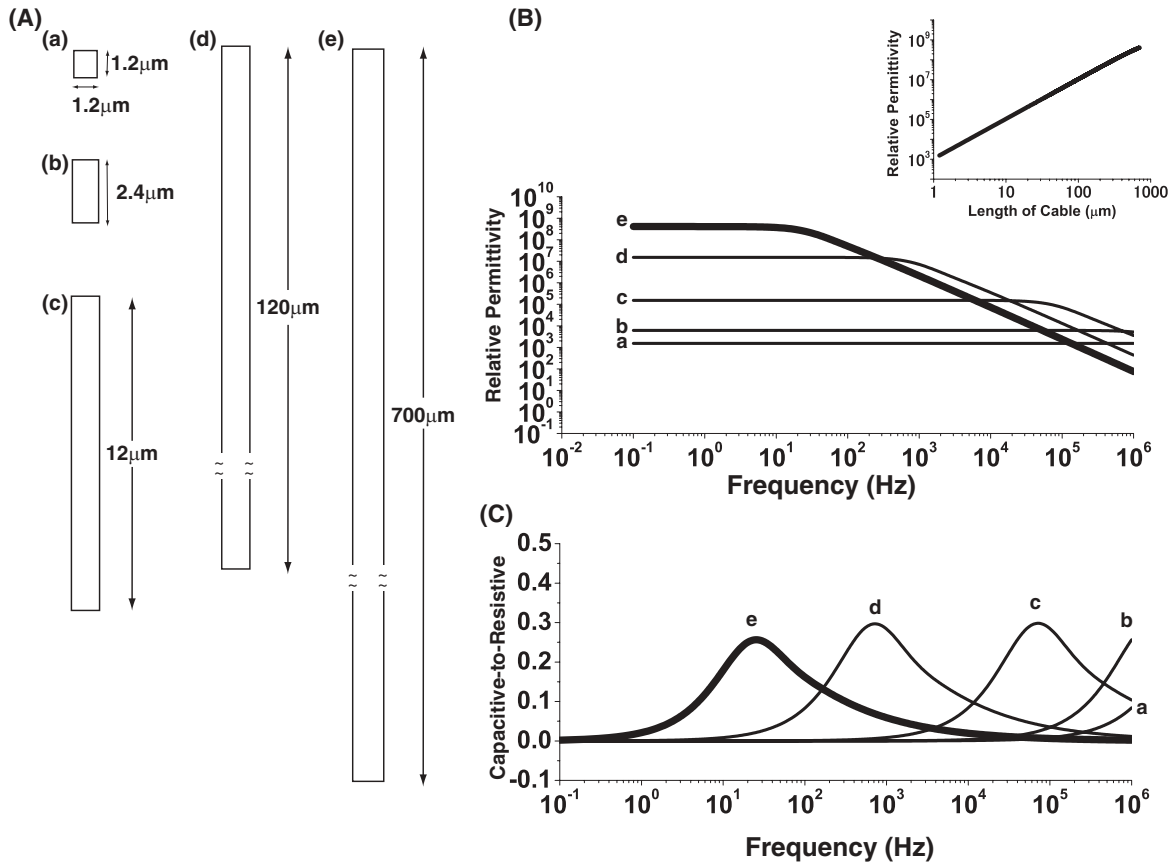


FIG. 5. Effect of cable length on the low-frequency dielectric dispersion. (A) Cables with various lengths, $L =$ (a) $1.2 \text{ } (\mu\text{m})$, (b) $2.4 \text{ } (\mu\text{m})$, (c) $12 \text{ } (\mu\text{m})$, (d) $120 \text{ } (\mu\text{m})$, (e) $700 \text{ } (\mu\text{m})$. In all cases, the diameter of the cable is $d = 1.2 \text{ } (\mu\text{m})$, and the diameter of the extracellular space is $d_{\text{ext}} = 1.2d$, and there is no shunt. (B) The relative permittivity for each length of the cable. Inset: The relative permittivity as a function of the length of the cable at 1 Hz. (C) The relative permittivity for each length of the cable. The bold curves (e) in (B) and (C) have the same identifications as broken curves in Figs. 4(A) and 4(D). The relative permittivity at 1 Hz increases with cable length in accordance with a power law.

B. Our model is an extreme case of Maxwell-Wagner dispersion

Our model is essentially an extension of the interfacial polarization theory (Maxwell-Wager-Sillars theory) [7,13] developed to understand β dispersion. The interfacial polarization theory accounts for the dielectric dispersion of suspensions of particles or cells as a phenomenon due to charging at the interface between materials with different permittivities, not due to the properties of the bulk phase of the materials. Although that theory was intended to model β dispersion, i.e., dispersion in the range 1 kHz–1 MHz, Takashima extended it and has shown that the dispersion of a suspension of ellipsoid particles depends on the axial ratio, finding that the permittivity in the low-frequency range increases with this ratio (pp. 162–168 in Ref. [13]). In that study, he solved the Laplace equation in ellipsoidal coordinates with several assumptions and found only a modest change in the permittivity due to a modest change in morphology. In line with this calculation, Asami has shown by numerical calculations that the permittivity of a cell suspension in the low-frequency region increases as the cells become increasingly elongated [14]. The present study is an attempt to elucidate the electrical properties of tissue in which an extremely elongated cell

is surrounded by an extracellular medium by solving cable equations for a cable of finite length. Thus, our model is an extreme case of Maxwell-Wagner dispersion.

The model used in the present study is too simplistic to estimate effective permittivity and conductivity of real tissue because there are mixtures of neurites with different length and orientations in real brain tissue and the electric field may not necessarily be parallel to the axis of the major neurites. Some of the neurites may not be as long as the model cable used in this study and the electric field may be perpendicular to the neurites. Recently, Bedard *et al.* proposed mechanisms for low-frequency dispersion [41–43]. Their theory is a synthesis of the interfacial polarization theory and the counterion polarization theory [15,44,45]. Making several assumptions, they attempted to find parameter values that would account for the experimental dispersion data reported by Gabriel *et al.* in the range of α dispersion. According to Grosse and Foster, the time constant of the dispersion, $\tau (= \epsilon/\sigma)$, is related to the radius R and the diffusion coefficient of the responsible ion D as

$$\tau = \frac{R^2}{D}. \quad (38)$$

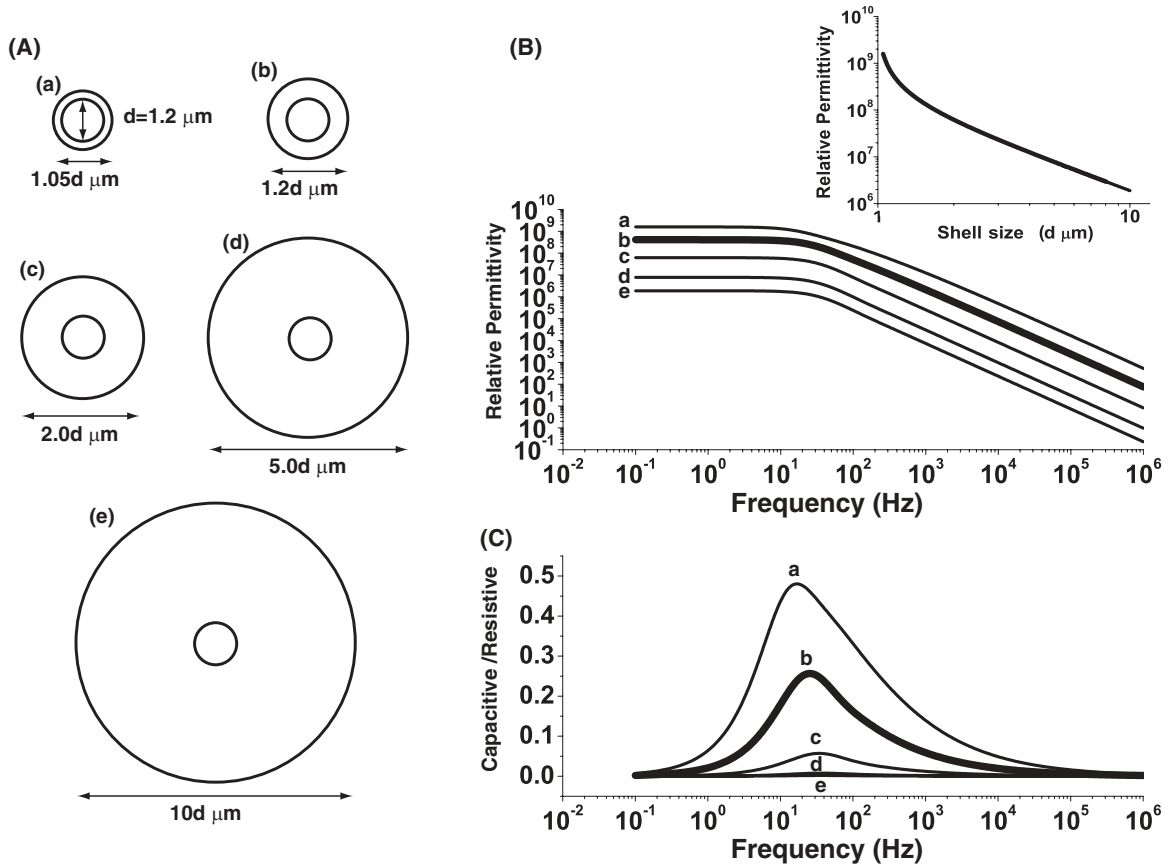


FIG. 6. Effect of the diameter of the extracellular space on the low-frequency dielectric dispersion. (A) The extracellular space with various diameters, $d_{ext} =$ (a) $1.05d$ (μm), (b) $1.2d$ (μm), (c) $2d$ (μm), (d) $5d$ (μm), (e) $10d$ (μm). In all cases, the diameter of the cable is $d = 1.2$ (μm), and there is no shunt. (B) The relative permittivity for each diameter. Inset: The relative permittivity as a function of the diameter at 1 Hz. (C) The relative permittivity for each diameter. The bold curves (b) in (B) and (C) have the same identifications as the broken curves in Figs. 4(A) and 4(D). The relative permittivity at 1 Hz decreases with diameter of the extracellular space in accordance with a power law.

For $R = 1$ (μm), τ given by this relation is 1 (msec), while for $R = 100$ (μm), it is 10 (sec). On the basis of those results, it appears that the counterion polarization theory may be useful for modeling the dielectric dispersion in the range 1 Hz–1 kHz for the direction perpendicular to the neurites, but the time constant is much too large to account for the dispersion in the direction parallel to the neurites. Although our model does not take the diffusion of ions into consideration, it yields results consistent with the experimental dispersion data obtained by Gabriel *et al.* Because brain tissue is dense with neurites with various length and orientation, both the counterion polarization mechanism and polarization due to long passive cables may be necessary to understand the electrical properties of the bulk brain tissue.

C. A large permittivity and a non-negligible capacitive current may be consistent with weak low-pass filter characteristics

Figure 3(B) elucidates the filtering characteristics of our model. It is seen that in both the cases of a passive uniform cable and of a cable with a shunt at one end there are weak low-pass characteristics, but the amplitude drops by only 1.7 dB as the frequency increases from 1 Hz to 0.5 kHz. This value is comparable to that reported in Logothesis *et al.*, specifically, a 1.9 dB drop in the cortical resistance as the

frequency increases from 10 Hz to 5 kHz [9]. Based on this experimentally measured frequency dependence of cortical resistance, Logothesis *et al.* concluded that “the cortical tissue has the properties of a simple ohmic conductor.” In our study, however, we found that the capacitive component of the extracellular current can be significant in comparison with the resistive component in the frequency range 1 Hz–1 kHz, yet the tissue possesses only weak low-pass filtering characteristics (Fig. 3). We now argue that these features are consistent with the strong dielectric dispersion. Let us consider the situation in which there exists only a single relaxation process. Then the permittivity and the conductivity should depend on the frequency in accordance with the following Debye equations [46]:

$$\epsilon = \epsilon_0 + \frac{\epsilon_s - \epsilon_0}{1 + \omega^2\tau^2}, \tag{39}$$

$$\sigma = \frac{(\epsilon_s - \epsilon_0)\omega^2\tau}{1 + \omega^2\tau^2}. \tag{40}$$

If we choose $\epsilon_s = 10^{13} \times \epsilon_0$ and $\tau = 4$ (sec), we obtain frequency dependencies of the permittivity and the conductance that are similar to those of the system in the model in our study [Fig. 7(A)]. As shown in Figs. 7(A) and 7(B), in both models the impedance exhibits no low-pass filtering properties,

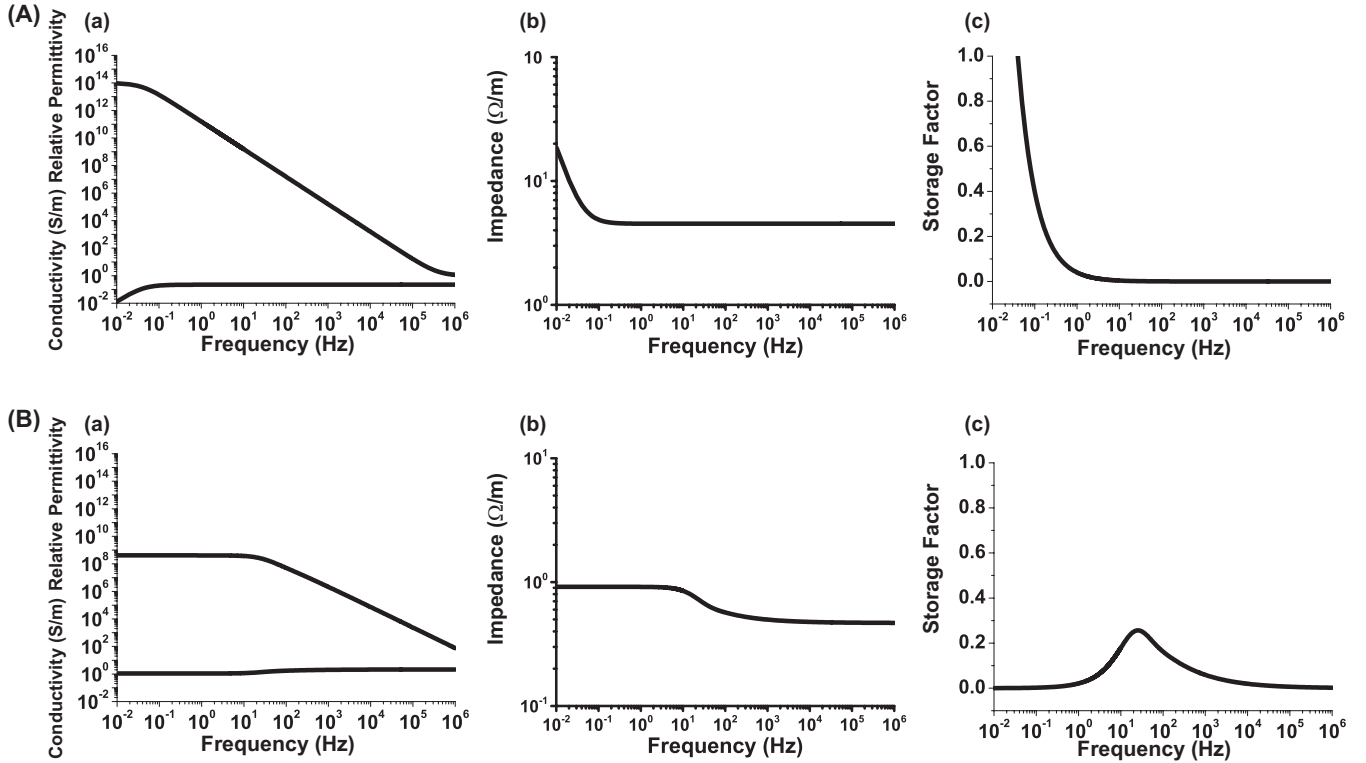


FIG. 7. Comparison between dielectric relaxation of a cable and simple Debye relaxation. (A) Simple Debye relaxation. (a) Relative permittivity (\cdot) and conductivity (S/m). (B) Impedance per unit length (Ω/m). (c) Storage factor (\cdot). (B) Dielectric relaxation of the cable. The curves marked “a,” “b,” and “c” represent those of the cable. With $\epsilon_s = 10^{13} \times \epsilon_0$ and $\tau = 4$ (sec), the Debye equation gives frequency dependencies of the permittivity and the conductivity similar to those of the cable, and it exhibits weak low-pass filter characteristics. In both the models, an extremely large permittivity and capacitive current in the low-frequency region can coexist with weak low-pass filter characteristics.

despite the significant magnitude of the capacitive current in the low-frequency range. The counterion model developed by Bedard *et al.* predicts low-pass filtering characteristics that are stronger than those observed by Logothetis *et al.*, who found a weak frequency dependence of the impedance in the brain tissues of monkey. Bedard *et al.* attributed this discrepancy to the saturation of the voltage at the electrodes used in the measurements. By contrast, our model does not predict such strong low-pass filtering characteristics. Thus, it allows for the simultaneous existence of a very large permittivity, a non-negligible capacitive current, and weak low-pass filter characteristics without the need for any kind of auxiliary arguments. These kinds of arguments are not necessary in our model because we think that very large permittivity and a non-negligible amount of capacitive current can be consistent with weak low-pass filter characteristics.

D. CSD analysis taking tissue permittivity into account

The current source density (CSD) analysis was developed [47,48] for analyzing the LFP. It has been used to estimate the location and timing of the source of the membrane current that generates the field potentials. In conventional CSD analysis, the extracellular space is assumed to be purely resistive. We have recently derived a general formula for the CSD analysis by which CSD in biological tissue [$I_{\text{CSD}}(x, \omega)$] with frequency-dependent permittivity [$\epsilon(x, \omega)$] and conductivity [$\sigma(x, \omega)$] can be obtained from the extracellular potential [$V_{\text{ext}}(x, \omega)$] [49].

The formula is as follows:

$$I_{\text{CSD}}(x, t) = (2\pi) \int \nabla \cdot [\sigma(x, \omega) + j\omega\epsilon(x, \omega)] \times [-\nabla V_{\text{ext}}(x, \omega)] e^{j\omega t} d\omega. \quad (41)$$

If the capacitive-to-resistive ratio of the current (i.e., the storage factor, $2\pi f\epsilon/\sigma$) is small enough, then we can ignore the capacitive component in the formula to obtain the conventional formula for CSD analysis. If the ratio is not small in the frequency range of interest, however, we need to take the permittivity into account in the CSD analysis. In practical measurements of LFP in performing CSD analysis, the distances between the recording points are usually 100–200 microns and the distances between sink and source are typically 100–300 microns. In Fig. 5, the model with the cable length of 120 microns shows high effective permittivity in the low-frequency range and significant capacitive-to-resistive ratio in the frequency range relevant in physiological measurements suggesting that permittivity of tissue may need to be considered in analyzing the sink-source pair with a distance as short as 120 microns. Because the frequency range the neuroscientists are interested in most is the range in which the permittivity is high and the capacitive-to-resistive ratio can be significant, we should not hastily ignore extracellular capacitive current.

ACKNOWLEDGMENTS

We thank Dr. J. Riera for suggesting that we examine the influence of cable properties on the dielectric properties of brain tissue, and we thank Dr. K. Asami for helpful discussions and comments on our study. This work was supported by grants from the Ministry of Education, Culture, Sports, Science and Technology of Japan (Grant No. 19300096 for H. Miyakawa, Grant No. 23500375 for T. Aonishi) and a Grant-in-Aid for Japan Society for the Promotion of Science (JSPS) Fellows (Grant No. 22-8010 for H. Monai).

APPENDIX: DERIVATION OF ANALYTICAL SOLUTION

Generally, the extracellular potential in the mean field model, depicted in Fig. 1(B), is indefinite, because the extracellular medium is not connected to a ground. However, if the stimuli are induced by an anode and a cathode, either electrode can be regarded as the ground because the sum of the stimulus currents entering and exiting the circuit is zero. Thus, the extracellular potential can be defined in this case.

To derive analytic solutions of the extracellular potential, we go through the following steps. In the first step, to avoid the indefiniteness of the extracellular potential in general situations, we extend this mean field model to a model consisting of N identical cables mutually coupled only through a single one-dimensional resistive extracellular space connected to a ground with conductance \tilde{g}_D [Fig. 8(A)]. When $\tilde{g}_D = 0$, this extended model is equivalent to the original mean field model. The extended mean field model can be exactly reduced to a single cable model connected to the ground with conductance \tilde{g}_D/N [Fig. 8(B)]. When $\tilde{g}_D = 0$, this equivalent single cable model becomes equivalent to the single cable model depicted in Fig. 1(C). In the next step, we derive an

approximate analytical solution to a single cable model that is equivalent to the extended mean field model in response to an extracellular stimulus created by the anode and the cathode. This approximate solution approaches an exact one when \tilde{g}_D is sufficiently small. In the final step, we confirm that in the limit $\tilde{g}_D \rightarrow 0$, the extracellular potential can be defined if stimuli are created by the anode and the cathode. In conclusion, we obtain analytical solutions for the extracellular potential in the original mean field model shown in Fig. 1(B).

1. Extracellular medium connected to ground

We extend the mean field model, depicted in Fig. 1(B) to a model in which the N identical cables are mutually coupled only through a single one-dimensional resistive extracellular space connected to a ground with conductance \tilde{g}_D as shown in Fig. 8(A). By connecting the extracellular medium to the ground, we can uniquely define the extracellular potential relative to the ground.

Kirchhoff's first law yields the following equations for the intracellular potential $V_{in}^k(x,t)$ of cable k ($k = 1, \dots, N$) and the extracellular potential $V_{ext}(x,t)$:

$$\frac{1}{r_{in}} \sum_{k=1}^N \frac{\partial^2 V_{in}^k(x,t)}{\partial x^2} = -\frac{1}{\tilde{r}_{ext}} \frac{\partial^2 V_{ext}(x,t)}{\partial x^2} + \tilde{g}_D V_{ext}(x,t), \tag{A1}$$

$$\begin{aligned} \frac{1}{r_{in}} \frac{\partial^2 V_{in}^k(x,t)}{\partial x^2} &= C_{mem} \frac{\partial [V_{in}^k(x,t) - V_{ext}(x,t)]}{\partial t} \\ &+ \frac{1}{r_{mem}} [V_{in}^k(x,t) - V_{ext}(x,t)], \end{aligned} \tag{A2}$$

$(k = 1, \dots, N).$

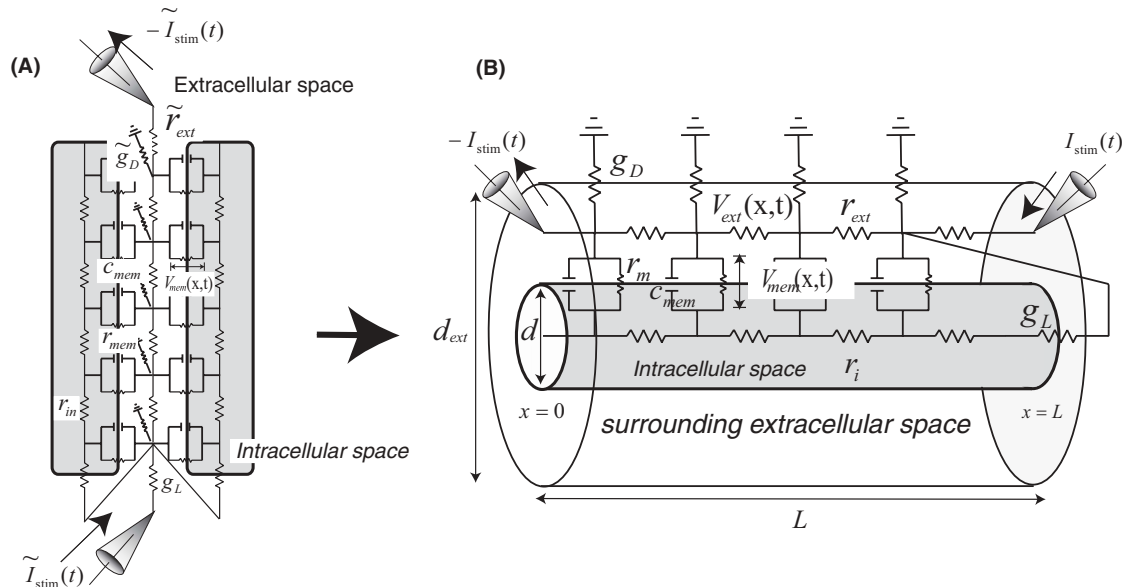


FIG. 8. (A) Extended mean field consisting of identical passive cables and a purely resistive extracellular medium connected to the ground with conductance \tilde{g}_D . By connecting extracellular media to the ground conductance \tilde{g}_D , we can determine the value of the extracellular potential V_{ext} relative to the ground. When $\tilde{g}_D = 0$, this model is equivalent to the original mean field model shown in Fig. 1(B). (B) Single cable model equivalent to the extended mean field model. When $g_D = 0$, this model is equal to the single cable model equivalent to the original mean field model [Fig. 1(C)].

Because identical cables do not interact directly but only through the single one-dimensional resistive extracellular space, N identical cables have the same membrane potential: $V_{\text{in}}^k(x, t) = V_{\text{in}}(x, t)$. Under this condition, defining $V_{\text{mem}}(x, t)$ as $V_{\text{in}}(x, t) - V_{\text{ext}}(x, t)$, Eqs. (A1) and (A2) can be rewritten as

$$c_{\text{mem}} \frac{\partial V_{\text{mem}}(x, t)}{\partial t} = \frac{1}{r_{\text{in}} + N\tilde{r}_{\text{ext}}} \frac{\partial^2 V_{\text{mem}}(x, t)}{\partial x^2} - \frac{1}{r_{\text{mem}}} V_{\text{mem}}(x, t) + \frac{\tilde{r}_{\text{ext}} \tilde{g}_D}{r_{\text{in}} + N\tilde{r}_{\text{ext}}} V_{\text{ext}}(x, t), \quad (\text{A3})$$

$$-\frac{\partial^2 V_{\text{mem}}(x, t)}{\partial x^2} = \frac{r_{\text{in}} + N\tilde{r}_{\text{ext}}}{N\tilde{r}_{\text{ext}}} \frac{\partial^2 V_{\text{ext}}(x, t)}{\partial x^2} - \frac{\tilde{g}_D}{N} r_{\text{in}} V_{\text{ext}}(x, t). \quad (\text{A4})$$

The last terms on the right-hand side of Eqs. (A3) and (A4) represent the effect of the connection to the ground. When $\tilde{g}_D = 0$, Eqs. (A3) and (A4) are equal to Eqs. (4) and (5).

In the extended model, we use the same boundary conditions as Eqs. (6) and (7). As mentioned above, in the mean field model, N identical cables have the same membrane potential. Applying Eq. (3) to those boundary conditions and subtracting the boundary conditions for the intracellular potential from those for the extracellular potential, we obtain the boundary conditions for the membrane potential and the extracellular potential:

$$\left. \frac{\partial V_{\text{mem}}(x, t)}{\partial x} \right|_{x=0} = \tilde{r}_{\text{ext}} \tilde{I}_{\text{stim}}(t), \quad (\text{A5})$$

$$\left. \frac{\partial V_{\text{mem}}(x, t)}{\partial x} \right|_{x=L} = \tilde{r}_{\text{ext}} \tilde{I}_{\text{stim}}(t) - (r_{\text{in}} + N\tilde{r}_{\text{ext}}) g_L V_{\text{mem}}(L, t),$$

$$\left. \frac{\partial V_{\text{ext}}(x, t)}{\partial x} \right|_{x=0} = -\tilde{r}_{\text{ext}} \tilde{I}_{\text{stim}}(t), \quad (\text{A6})$$

$$\left. \frac{\partial V_{\text{ext}}(x, t)}{\partial x} \right|_{x=L} = -\tilde{r}_{\text{ext}} \tilde{I}_{\text{stim}}(t) + N\tilde{r}_{\text{ext}} g_L V_{\text{mem}}(L, t).$$

Here, $\tilde{I}_{\text{stim}}(t)$ is a time-varying stimulus current created by the anode and cathode pair located in the extracellular space. If $g_L = 0$, the cable is sealed at both ends and symmetrical with respect to a direction along its axis.

Generally, it is difficult to solve differential equations with such time-varying boundary conditions. To avoid this difficulty, we consider a physically equivalent system in which there is no complicated time dependence of the boundary conditions but the effect is accounted for through the introduction of current densities in the intracellular and extracellular media. Through this mathematical manipulation, Eqs. (A3) and (A4) can be rewritten as

$$r_{\text{mem}} c_{\text{mem}} \frac{\partial V_{\text{mem}}(x, t)}{\partial t} = \frac{r_{\text{mem}}}{r_{\text{in}} + N\tilde{r}_{\text{ext}}} \frac{\partial^2 V_{\text{mem}}(x, t)}{\partial x^2} - V_{\text{mem}}(x, t) + \frac{r_{\text{mem}} \tilde{r}_{\text{ext}} \tilde{g}_D}{r_{\text{in}} + N\tilde{r}_{\text{ext}}} V_{\text{ext}}(x, t) - \frac{r_{\text{mem}} \tilde{r}_{\text{ext}}}{r_{\text{in}} + N\tilde{r}_{\text{ext}}} \tilde{I}_{\text{cd}}(x, t), \quad (\text{A7})$$

$$\begin{aligned} & \frac{r_{\text{mem}}}{N\tilde{r}_{\text{ext}}} \frac{\partial^2 V_{\text{ext}}(x, t)}{\partial x^2} - r_{\text{in}} \frac{\tilde{g}_D}{N} \frac{r_{\text{mem}}}{r_{\text{in}} + N\tilde{r}_{\text{ext}}} V_{\text{ext}}(x, t) \\ &= -\frac{r_{\text{mem}}}{r_{\text{in}} + N\tilde{r}_{\text{ext}}} \frac{\partial^2 V_{\text{mem}}(x, t)}{\partial x^2} - \delta(x - L) r_{\text{mem}} g_L V_{\text{mem}}(L, t) \\ & \quad - \frac{r_{\text{mem}}}{r_{\text{in}} + N\tilde{r}_{\text{ext}}} r_{\text{in}} \tilde{I}_{\text{cd}}(x, t), \end{aligned} \quad (\text{A8})$$

where $\tilde{I}_{\text{cd}}(x, t) = \tilde{I}_{\text{stim}}(t)[\delta(x - \Delta x) - \delta(x - L + \Delta x)]$. $\delta(t)$ is the Dirac δ function, and Δx is an infinitesimal distance along the cable. For this system, the boundary conditions are

$$\left. \frac{\partial V_{\text{mem}}(x, t)}{\partial x} \right|_{x=0} = 0, \quad (\text{A9})$$

$$\left. \frac{\partial V_{\text{mem}}(x, t)}{\partial x} \right|_{x=L} = -(r_{\text{in}} + N\tilde{r}_{\text{ext}}) g_L V_{\text{mem}}(L, t),$$

$$\left. \frac{\partial V_e(x, t)}{\partial x} \right|_{x=0} = 0, \quad \left. \frac{\partial V_e(x, t)}{\partial x} \right|_{x=L} = 0. \quad (\text{A10})$$

These are the same as Eqs. (13) and (14).

2. Equivalent single cable model within an extracellular medium connected to ground

Replacing $N\tilde{r}_{\text{ext}}$, \tilde{g}_D/N , $\tilde{I}_{\text{stim}}(t)/N$ and $\tilde{I}_{\text{cd}}(x, t)/N$ with r_{ext} , g_D , $I_{\text{stim}}(t)$, and $I_{\text{cd}}(x, t)$ respectively, the system described by Eqs. (A7)–(A10) becomes equivalent to a model consisting of a single cable and a surrounding extracellular medium connected to the ground [Fig. 8(B)]. From Eq. (10), the newly introduced current density $I_{\text{cd}}(x, t)$ becomes $I_{\text{cd}}(x, t) = I_{\text{stim}}(t)[\delta(x - \Delta x) - \delta(x - L + \Delta x)]$. $N\tilde{r}_{\text{ext}}$ can be mathematically interpreted as the resistivity of one of N extracellular subspaces into which the extracellular space of the extended mean field model is equally divided, $\tilde{I}_{\text{stim}}(t)/N$ can be interpreted as the value of the stimulus current flowing through one of the N extracellular subspaces, and \tilde{g}_D/N can be interpreted as the ground conductance equally divided into N extracellular subspaces. Therefore, the extended mean field model can be separated into N isolated elements, given by

$$\begin{aligned} \tau_{\text{mem}} \frac{\partial V_{\text{mem}}(x, t)}{\partial t} &= \lambda_{\text{mem}}^2 \frac{\partial^2 V_{\text{mem}}(x, t)}{\partial x^2} - V_{\text{mem}}(x, t) \\ & \quad + \lambda_{\text{mem}}^2 r_{\text{ext}} g_D V_{\text{ext}}(x, t) - \lambda_{\text{mem}}^2 r_{\text{ext}} I_{\text{cd}}(x, t), \end{aligned} \quad (\text{A11})$$

$$\begin{aligned} & \frac{r_{\text{mem}}}{r_{\text{ext}}} \frac{\partial^2 V_{\text{ext}}(x, t)}{\partial x^2} - \lambda_{\text{mem}}^2 r_{\text{in}} g_D V_{\text{ext}}(x, t) \\ &= -\lambda_{\text{mem}}^2 \frac{\partial^2 V_{\text{mem}}(x, t)}{\partial x^2} - \delta(x - L) r_{\text{mem}} g_L V_{\text{mem}}(L, t) \\ & \quad - \lambda_{\text{mem}}^2 r_{\text{in}} I_{\text{cd}}(x, t), \end{aligned} \quad (\text{A12})$$

where λ_{mem} and τ_{mem} are the space constant (cm) and time constant (msec), defined by

$$\lambda_{\text{mem}} = \sqrt{\frac{r_{\text{mem}}}{r_{\text{in}} + r_{\text{ext}}}} \quad \text{and} \quad \tau_{\text{mem}} = r_{\text{mem}} c_{\text{mem}}. \quad (\text{A13})$$

When $g_D = 0$, Eqs. (A11) and (A12) are equal to Eqs. (15) and (16).

The boundary conditions Eqs. (A9) and (A10) become

$$\left. \frac{\partial V_{\text{mem}}(x,t)}{\partial x} \right|_{x=0} = 0, \quad (A14)$$

$$\left. \frac{\partial V_{\text{mem}}(x,t)}{\partial x} \right|_{x=L} = -(r_{\text{in}} + r_{\text{ext}})g_L V_{\text{mem}}(L,t),$$

$$\left. \frac{\partial V_e(x,t)}{\partial x} \right|_{x=0} = 0, \quad \left. \frac{\partial V_e(x,t)}{\partial x} \right|_{x=L} = 0. \quad (A15)$$

These are the same as Eqs. (17) and (18).

3. Approximate solution of the single cable model equivalent to the extended mean field model

To derive an analytic solution to the single cable model equivalent to the extended mean field model, we assume g_D in Eq. (A11) to be negligibly small and remove the third term on the right-hand side in Eq. (A11):

$$\tau_{\text{mem}} \frac{\partial V_{\text{mem}}(x,t)}{\partial t} = \lambda_{\text{mem}}^2 \frac{\partial^2 V_{\text{mem}}(x,t)}{\partial x^2} - V_{\text{mem}}(x,t) - \lambda_{\text{mem}}^2 r_{\text{ext}} I_{\text{cd}}(x,t). \quad (A16)$$

Here, we derive a solution to Eqs. (A12) and (A16) under the boundary conditions appearing in Eqs. (A14) and (A15). This solution provides approximate values for the membrane and the extracellular potentials in the extended model if g_D is sufficiently small.

Because the membrane potential can be calculated independently from the extracellular potential under this approximation, the right-hand side term of Eq. (A12), consisting of the membrane potential $V_{\text{mem}}(x,t)$ and the stimulus current $I_{\text{stim}}(t)$, can be regarded as the current density independently given along the extracellular medium

$$\frac{r_{\text{mem}}}{r_{\text{ext}}} \frac{\partial^2 V_{\text{ext}}(x,t)}{\partial x^2} - \lambda_{\text{mem}}^2 r_{\text{in}} g_D V_{\text{ext}}(x,t) = -I_T(x,t), \quad (A17)$$

$$I_T(x,t) = \lambda_{\text{mem}}^2 r_{\text{in}} I_{\text{cd}}(x,t) + \lambda_{\text{mem}}^2 \frac{\partial^2 V_{\text{mem}}(x,t)}{\partial x^2} + \delta(x-L)r_{\text{mem}}g_L V_{\text{mem}}(L,t). \quad (A18)$$

By substituting Eq. (19) into Eq. (A18), we can express $I_T(x,t)$ as a Fourier series expansion with eigenfunctions $\{\varphi_n(x)\}$ satisfying the leaky boundary condition appearing in Eq. (A14):

$$I_T(x,t) = \lambda_{\text{mem}}^2 r_{\text{in}} I_{\text{cd}}(x,t) - \lambda_{\text{mem}}^2 \sum_{n=0}^{\infty} A_n \mu_n^2 \varphi_n(x) \times \int_0^t dt' \exp\left(-\frac{t-t'}{\kappa_n}\right) I_{\text{stim}}(t') + \delta(x-L)r_{\text{mem}}g_L \sum_{n=0}^{\infty} A_n \varphi_n(L) \times \int_0^t dt' \exp\left(-\frac{t-t'}{\kappa_n}\right) I_{\text{stim}}(t'). \quad (A19)$$

The Green's function of Eq. (A17) under the reflecting boundary condition at both ends [Eq. (A15)] is

$$G_e(x,x',t,t') = \delta(t-t') \frac{2}{L} \sum_{m=-\infty}^{\infty} \frac{\cos\left(\frac{n\pi}{L}x'\right)}{\frac{r_{\text{mem}}}{r_{\text{ext}}}\left(\frac{m\pi}{L}\right)^2 + \lambda_{\text{mem}}^2 r_{\text{in}} g_D} \times \cos\left(\frac{n\pi}{L}x\right), \quad (A20)$$

where x and t are the observation point and time for an impulse response, and x' and t' are the position and time of an impulse input. This Green's function has a form of Fourier series expansion with the eigenfunctions $\{\cos(\frac{n\pi}{L}x)\}$ satisfying the reflecting boundary condition appearing in Eq. (A15).

Assuming that the initial condition of the extracellular potential is $V_{\text{ext}}(x,0) = 0$, by convolving Eq. (A19) with Eq. (A20), we can derive an analytical solution of the extracellular potential. This convolution operation requires taking the inner products between two eigenfunctions satisfying different boundary conditions:

$$\int_0^L dx \cos\left(\frac{n\pi x}{L}\right) \varphi_k(x) = \begin{cases} \frac{\mu_k \cos(\pi n) \sin(\mu_k L)}{\mu_k^2 - \left(\frac{n\pi}{L}\right)^2} & (g_L > 0) \\ \frac{L}{2} \delta_{nk} & (g_L = 0) \end{cases},$$

where δ_{nk} is the Kronecker δ .

Finally, we obtain an approximate solution to the extracellular potential in the extended model:

$$V_{\text{ext}}(x,t) = \lambda_{\text{mem}}^2 r_{\text{in}} I_{\text{stim}}(t) \frac{2}{L} \sum_{m=1}^{\infty} \frac{1 - \cos(m\pi)}{\frac{r_{\text{mem}}}{r_{\text{ext}}}\left(\frac{m\pi}{L}\right)^2 + \lambda_{\text{mem}}^2 r_{\text{in}} g_D} \cos\left(\frac{m\pi}{L}x\right) + r_{\text{mem}}g_L \frac{2}{L} \sum_{m=1}^{\infty} \frac{\cos(m\pi)}{\frac{r_{\text{mem}}}{r_{\text{ext}}}\left(\frac{m\pi}{L}\right)^2 + \lambda_{\text{mem}}^2 r_{\text{in}} g_D} \times \cos\left(\frac{m\pi}{L}x\right) \sum_{n=0}^{\infty} \frac{A_n \varphi_n(L) \left(\frac{m\pi}{L}\right)^2}{\left(\frac{m\pi}{L}\right)^2 - \mu_n^2} \int_0^t dt' \exp\left(-\frac{t-t'}{\kappa_n}\right) I_{\text{stim}}(t'). \quad (A21)$$

When $g_L = 0$ (sealed-end case), this analytical solution takes a simple form:

$$V_{\text{ext}}(x,t) = \lambda_{\text{mem}}^2 r_{\text{in}} I_{\text{stim}}(t) \frac{2}{L} \sum_{m=1}^{\infty} \frac{1 - \cos(m\pi)}{\frac{r_{\text{mem}}}{r_{\text{ext}}}\left(\frac{m\pi}{L}\right)^2 + \lambda_{\text{mem}}^2 r_{\text{in}} g_D} \cos\left(\frac{m\pi}{L}x\right) - \lambda_{\text{mem}}^2 \sum_{m=1}^{\infty} \frac{A_m \left(\frac{m\pi}{L}\right)^2}{\frac{r_{\text{mem}}}{r_{\text{ext}}}\left(\frac{m\pi}{L}\right)^2 + \lambda_{\text{mem}}^2 r_{\text{in}} g_D} \cos\left(\frac{m\pi}{L}x\right) \int_0^t dt' \exp\left(-\frac{t-t'}{\kappa_m}\right) I_{\text{stim}}(t'). \quad (A22)$$

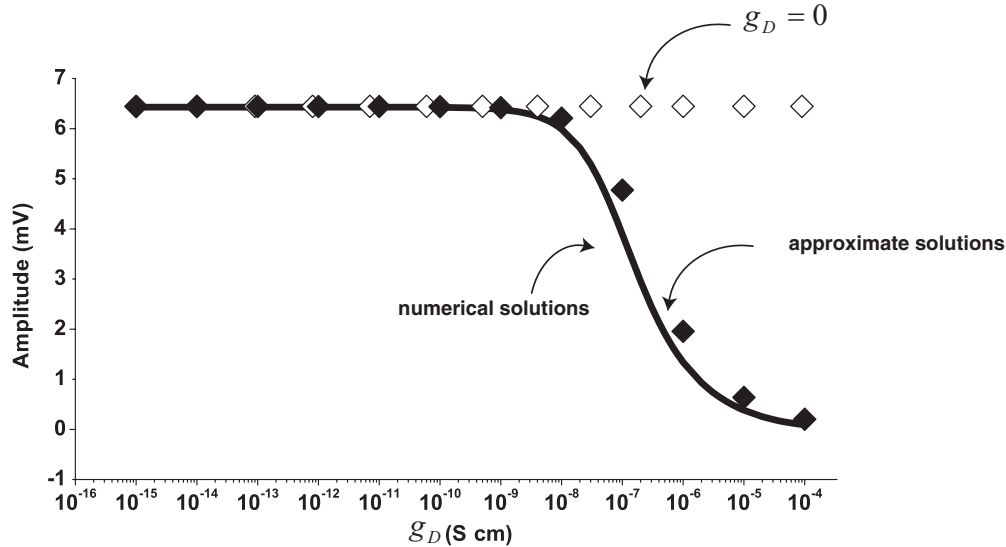


FIG. 9. Comparison between the analytical and the numerical solutions when $g_D \neq 0$. We plot the extracellular potential (mV) in steady state when applying a direct-current (dc) stimulus as a function of g_D varying from $g_D = 1.0 \times 10^{-15}$ to 1.0×10^{-4} (S cm). The solid curves represent the direct numerical solutions of the single cable model equivalent to the extended mean field model, which are obtained by employing the implicit method for Eqs. (A11) and (A12) with the boundary conditions [Eqs. (A14) and (A15)]. The close diamonds represent values of the approximate analytical solution represented by Eq. (A21) when $g_D \neq 0$, and the open diamonds denote values of the analytical solution represented by Eq. (24) [i.e., Eq. (A21) when $g_D = 0$]. The infinite series contained in Eq. (A21) were truncated at $n = 1000$.

Equations (A21) and (A22) are Fourier series expansions with the eigenfunctions, $\{\cos(\frac{n\pi x}{L})\}$. When the cable is stimulated by the extracellular currents, $I_{\text{stim}}(t)$ and $-I_{\text{stim}}(t)$, that are created by the anode and the cathode in the extracellular space, the dc terms of the Fourier series in these equations become zero.

To verify the accuracy of the approximate solution, we compared it with a direct numerical solution of Eqs. (A11) and (A12) under the boundary conditions appearing in Eqs. (A14) and (A15) (calculated by the implicit method). Figure 9 shows those solutions in the steady state when applying a dc stimulus with various values of g_D . As g_D decreases, the approximate solution approaches the direct numerical solution.

4. In the limit $g_D \rightarrow 0$

Finally, we confirm that in the limit $g_D \rightarrow 0$, the extracellular potential can be defined if stimuli are created by the anode and the cathode in the extracellular space. Generally, the extracellular potential $V_{\text{ext}}(x, t)$ is indefinite when $g_D = 0$, because the extracellular medium is not connected to the ground. It is impossible to derive a general solution to the extracellular potential for any extracellular stimuli, because the dc term of the Fourier series in the Green's function

[Eq. (A20)] has a singular point at $g_D = 0$, reflecting no connection to the ground. However, as mentioned above, in the case that the dc terms of a Fourier series in Eqs. (A21) and (A22) become zero, the extracellular potential can be defined in the limit $g_D \rightarrow 0$, and thus we can obtain the analytical solution to the extracellular potential in the cable model depicted in Fig. 1(C) and expressed in Eq. (24). In this way, our derivation process is complete.

5. Numerical simulation

It is impossible to numerically solve Eqs. (15) and (16) under Eqs. (17) and (18) because of the indefiniteness inherent in solving the Poisson equation [Eq. (16)] under reflecting boundary conditions. Instead, by employing an implicit method, we can numerically solve the single cable model equivalent to the extended mean field model, i.e., Eqs. (A11) and (A12) under the boundary conditions [Eqs. (A14) and (A15)]. As shown in Fig. 9, the numerical solutions of the single cable model give values very close to the analytical solutions of the single cable equivalent model when g_D is sufficiently small. In this paper, the ground conductance is set to be $g_D = 1.0 \times 10^{-15}$ (S cm).

- [1] K. S. Cole and R. H. Cole, *J. Chem. Phys.* **9**, 341 (1941).
 [2] K. S. Cole and R. H. Cole, *J. Chem. Phys.* **10**, 98 (1942).
 [3] K. R. Foster and H. P. Schwan, in *Critical Reviews in Biomedical Engineering*, Vol. 17 (Begall House, New York, 1989), pp. 25–104.
 [4] H. P. Schwan and K. S. Cole, in *Bioelectricity: Alternating Current Admittance of Cells and Tissues*, Medical Physics,

- edited by O. Glasser, Vol. 3 (Yearbook Publishers, Inc., Chicago, 1960).
 [5] H. P. Schwan, in *Physical Techniques in Biological Research*, edited by W. L. Nastuk, Vol. 6 (Academic, New York, 1963), p. 323.
 [6] K. S. Cole, *Membranes, Ions and Impulses: A Chapter of Classical Biophysics*, Biophysics series, Vol. 1 (University

- of California Press, Berkeley and Los Angeles, Calif, 1968).
- [7] K. R. Foster and H. P. Schwan, *Crit. Rev. Biomed. Eng.* **17**, 25 (1989).
- [8] P. Nunez and R. Srinivasan, *Electric Fields of the Brain: The Neurophysics of EEG*, 2nd ed. (Oxford University Press, New York, 2005).
- [9] N. K. Logothetis, C. Kayser, and A. Oeltermann, *Neuron* **55**, 809 (2007).
- [10] C. Gabriel, S. Gabriel, and E. Corthout, *Phys. Med. Biol.* **41**, 2231 (1996).
- [11] S. Gabriel, R. W. Lau, and C. Gabriel, *Phys. Med. Biol.* **41**, 2251 (1996).
- [12] S. Gabriel, R. W. Lau, and C. Gabriel, *Phys. Med. Biol.* **41**, 2271 (1996).
- [13] S. Takashima, *Electrical Properties of Biopolymers and Membranes* (Adam Hilger, London, 1989).
- [14] K. Asami, *J. Phys. D: Appl. Phys.* **39**, 492 (2006).
- [15] G. Schwarz, *J. Phys. Chem.* **66**, 2636 (1962).
- [16] H. Monai, T. Omori, M. Okada, M. Inoue, H. Miyakawa, and T. Aonishi, *Biophys. J.* **98**, 524 (2010).
- [17] M. Bikson, M. Inoue, H. Akiyama, J. K. Deans, J. E. Fox, H. Miyakawa, and J. G. Jefferys, *J. Phys.* **557**, 175 (2004).
- [18] H. Akiyama, Y. Shimizu, H. Miyakawa, and M. Inoue, *Brain Res.* **1383**, 22 (2011).
- [19] G. Stuart and N. Spruston, *J. Neurosci.* **18**, 3501 (1998).
- [20] M. Inoue, Y. Hashimoto, Y. Kudo, and H. Miyakawa, *Eur. J. Neurosci.* **13**, 1711 (2001).
- [21] N. L. Golding, T. J. Mickus, Y. Katz, W. L. Kath, and N. Spruston, *J. Phys.* **568**, 69 (2005).
- [22] T. Omori, T. Aonishi, H. Miyakawa, M. Inoue, and M. Okada, *Brain Res.* **1125**, 199 (2006).
- [23] H. Bokil, N. Laaris, K. Blinder, M. Ennis, and A. Keller, *J. Neurosci.* **21**, RC173 (2001).
- [24] L. A. Cartee and R. Plonsey, *IEEE Trans. Biomed. Eng.* **39**, 76 (1992).
- [25] W. Rall, *Exp. Neurol.* **1**, 491 (1959).
- [26] M. Kawato, *J. Theor. Biol.* **111**, 149 (1984).
- [27] D. Durand, *Biophys. J.* **46**, 645 (1984).
- [28] G. Svirskis, A. Gutman, and J. Hounsgaard, *J. Neurophysiol.* **77**, 579 (1997).
- [29] N. Spruston and D. Johnston, *J. Neurophysiol.* **67**, 508 (1992).
- [30] J. M. Bekkers and C. F. Stevens, *J. Neurophysiol.* **75**, 1250 (1996).
- [31] G. Major, A. U. Larkman, P. Jonas, B. Sakmann, and J. J. Jack, *J. Neurosci.* **14**, 4613 (1994).
- [32] W. H. Press, S. A. Teukolsky, W. T. Vetterling, and B. P. Flannery, *Numerical Recipes 3rd Edition: The Art of Scientific Computing*, 3rd ed. (Cambridge University Press, Cambridge, England, 2007).
- [33] F. Rattay, *Neuroscience* **89**, 335 (1999).
- [34] C. Nicholson, in *Neuroglia*, edited by H. Kettenmann and B. R. Ransom (Oxford University Press, New York, 2004), pp. 387–397.
- [35] K. C. Chen and C. Nicholson, *Proc. Natl. Acad. Sci. USA* **97**, 8306 (2000).
- [36] R. G. Thorne and C. Nicholson, *Proc. Natl. Acad. Sci. USA* **103**, 5567 (2006).
- [37] D. Attwell, *Radiat Prot Dosimetry* **106**, 341 (2003).
- [38] R. Ventura and K. M. Harris, *J. Neurosci.* **19**, 6897 (1999).
- [39] J. Wolff, *Acta Neuropathol. Suppl* **4**, 33-9 (1968).
- [40] A. Reichenbach and H. Wolburg, in *Neuroglia*, 2nd ed., edited by H. Kettenmann and B. R. Ransom (Oxford University Press, New York, 2004), pp. 19–35.
- [41] C. Bedard, H. Kroger, and A. Destexhe, *Biophys. J.* **86**, 1829 (2004).
- [42] C. Bedard, H. Kroger, and A. Destexhe, *Phys. Rev. E* **73**, 051911 (2006).
- [43] C. Bedard and A. Destexhe, *Biophys. J.* **96**, 2589 (2009).
- [44] C. Grosse and K. R. Foster, *J. Phys. Chem.* **91**, 3073 (1987).
- [45] C. Grosse, *J. Phys. Chem.* **92**, 3905 (1988).
- [46] P. Debye, *Polar Molecules* (Chemical Catalog, New York, 1929).
- [47] C. Nicholson and J. A. Freeman, *J. Neurophysiol.* **38**, 356 (1975).
- [48] U. Mitzdorf, *Physiol Rev.* **65**, 37 (1985).
- [49] H. Miyakawa and T. Aonishi, [arXiv:1209.4722](https://arxiv.org/abs/1209.4722) [q-bio.NC].